1960

Inelastic lateral buckling of beams, Welded Continuous Frames and their Components, October 1960

T. V. Galambos

M. G. Lay

Welded Continuous Frames and Their Components

INELASTIC LATERAL BUCKLING OF BEAMS

by

Theodore V. Galambos

This work has been carried out as a part of an investigation sponsored jointly by the Welding Research Council and the Department of the Navy with funds furnished by the following:

American Institute of Steel Construction
American Iron and Steel Institute
Institute of Research, Lehigh University
Column Research Council (Advisory)
Office of Naval Research (Contract Nonr 610(03))
Bureau of Ships
Bureau of Yards and Docks

October 1960

Fritz Engineering Laboratory Report No. 205A.28

S Y N O P S I S

In this paper a method is proposed for the solution of the inelastic lateral buckling problem of as-rolled wide-flange beams subjected to equal end moments. The method is based on the determination of the reduction in the lateral and the torsional stiffnesses due to yielding. The effect of initial residual stresses is included in the calculations. An "exact" analytical procedure is worked out for several examples at first, and then a simplified formula is proposed which reduces the computational work considerably. Currently used empirical design procedures are checked against the results, and a possible modification of one of them is discussed.

TABLE OF CONTENTS

I. INTRODUCTION

A perfectly straight steel wide-flange beam which is subjected to bending moments about its strong axis (the x-x axis as shown in the inset of Fig. 1) will deflect in the plane of the applied moments as long as these moments are below a certain critical value. However, when the critical loading is reached, bifurcation of the equilibrium will take place, and failure due to lateral buckling is initiated by lateral deflection and twisting of the member.(1)(2)

The buckling of axially loaded columns is usually represented by so-called "column-curves", where the relationship between the length of the member and its critical load is plotted on a cartesian coordinate system. Similar relationships can be established for the lateral buckling of beams. A typical length versus critical moment curve is shown in Fig. 1 for a simply supported steel wide-flange beam subjected to equal end moments. This curve consists of the following three parts: (1) Portion CD represents classical elastic buckling(1); (2) Portion AB depicts the buckling behavior of a very short member for which it can be assumed that all fibers have been strained into the strain-hardening range(3), and (3) portion BC of the curve corresponds to buckling in the inelastic range. Buckling in this range takes place when some parts of the cross section are yielded, while other parts are still elastic. The strain-hardening and the elastic curves are typical Euler hyperbolas which do not intersect. The curve for inelastic buckling provides a transition between these two extreme idealizations.

In the ensuing report a method will be presented for the determination of the buckling strength in the inelastic range. The problem will be solved for the case of a simply supported as-rolled steel wide-flange beam subjected to equal end moments causing single curvature deformation. An analytically "exact" solution will be developed for a given average residual stress distribution. This solution will then be simplified for design application. Finally, the results will be compared with existing empirical approximations, and a possible design modification will be discussed.

I.1 PREVIOUS WORK

Of the three types of problems shown in Fig. 1, the problem of elastic lateral buckling has been investigated most thoroughly.* Solutions for the lateral buckling of beams in the strain-hardening range have been developed recently for structural steel wide-flange beams(3) and for rectangular beams made of a metal having a monotonically increasing stress-strain curve.(4) Inelastic lateral buckling solutions for steel beams of rectangular(5) and wide-flange(6) shape containing no residual stresses are available. In an unpublished report(7) the author has presented solutions for the determination of the inelastic lateral-torsional buckling strength of as-rolled wide-flange beam-columns. The following report is a summary and an extension of that work in Ref. 7 which pertains to the buckling of beams. This work differs from previous solutions in the fact that the reduction in beam stiffness due to early yielding caused by the residual stresses is included in the calculations.

---

*A discussion of this work can be found in Refs. 1 and 2. These references include extensive listings of the pertinent literature.

I.2 LATERAL BUCKLING IN THE INELASTIC RANGE

Schematic load-deflection curves for beams failing by lateral buckling in the inelastic range are shown in Fig. 2. The inset of Fig. 2a illustrates two possible deflection configurations into which any interior cross section of the beam may be deformed: For the first of these, the only deformation is the transverse deflection v. The beam is located directly below the undeflected cross section and in the plane of the applied moment. The second deflection configuration represents the buckled shape of the cross section. The corresponding deformations are the transverse deflection v, the lateral deflection u, and the twist β. Bifurcation of the equilibrium takes place when the cross section moves from its laterally undeflected deflection configuration to an infinitely close buckled deformation .

The curve in Fig. 2a shows the relationship between the applied end moment M_o and the transverse deflection v as M_o is increased from zero to its maximum value M_m. If no lateral buckling were to occur, the curve would increase monotonically until it would approach the fully plastic moment M_p as an asymptote (dashed curve). However, at the critical moment M_{cr} (where M_{cr} is above the elastic limit moment M_e for inelastic buckling) bifurcation of the equilibrium takes place, and the deflection curve deviates from its original course because of lateral buckling. The beam will still be able to support a small increase of moment to M_m, after which rapid unloading indicates failure.

The relationship between M_o and the lateral deflection u or the twisting angle β is illustrated in Fig. 2b. No lateral deflection or twist is present until the critical moment is reached. As the moment is increased above M_{cr}, these deformations will rapidly increase until M_m and thus failure is reached. In the case of small initial imperfections lateral deformations u and β will exist from the start of loading (see dot-dash curve in Fig. 2b).

The computation of the maximum moment for perfectly straight beams or for beams with small initial excentricities is quite complicated.[2] For this reason the moment causing initiation of lateral buckling will be used as a lower bound to the maximum moment. This moment is computed on the basis that at buckling no previously yielded fibers will unload elastically and that additional bending is resisted by the unyielded elastic core of the member. The critical moment M_{cr} corresponds to the critical or "tangent modulus" load of axially loaded columns failing in the inelastic range.[1] Just as the tangent modulus load is taken as the critical load for axially loaded columns, here the moment causing initiation of buckling is taken as the critical moment at which the structural usefulness of the beam is exhausted. This assumption usually results in only a small conservative error.

II. DEVELOPMENT OF THE THEORY

II.1 ASSUMPTIONS

The following assumptions underlie the subsequent theoretical derivations:

(1) No external lateral forces are applied to the beam between supports.

(2) The beam is initially straight and free of imperfections.

(3) The cross section retains its original shape during buckling (that is, local buckling is assumed to be not critical[8]).

(4) The ends of the beam may not translate or twist; however they are free to rotate laterally and the end sections are free to warp ("simply supported" end-conditions[1]).

(5) The applied end bending moments are equal, causing single curvature deformation about the strong axis of the beam (see inset of Fig. 1).

(6) The beams are as-rolled, ASTM-A7 steel wide-flange shapes. The idealized cross section is shown in Fig. 3 (fillets and variations of the flange thickness are neglected).

(7) The cross sectional and material properties are uniform along the whole length of the beam.

(8) The stress-strain diagram is as shown in Fig. 4. The material properties are assumed to be uniform over the cross section. The following standard values of these coefficients are used for computational purposes:

$$\sigma_y = 33 \text{ ksi}$$

$E = 30,000$ ksi

$E_{st} = 900$ ksi[8]

$G = 11,500$ ksi

$G_{st} = 2,400$ ksi[8]

(9) The assumed residual stress pattern is shown in Fig. 5.[9] These stresses are assumed constant across the thickness of each cross section element. The stress σ_{rc} is the maximum compressive stress at the tips of the flanges, and σ_{rt} is the maximum tensile residual stress. Consideration of equilibrium requires that the relationship between σ_{rc} and σ_{rt} be the following:[9]

$$\sigma_{rt} = \left[\frac{bt \quad \sigma_{rc}}{bt + w(d-2t)} \right] \quad \ldots . (1)$$

where b, t, w, and d are cross sectional dimensions defined in Fig. 3. A maximum compressive residual stress of $\sigma_{rc} = 0.3\,\sigma_y$ will be used for the numerical computations.[9]

II.2 THE BUCKLING EQUATION

The equation representing the critical combination of length and end moment for simply supported wide-flange beams under uniform moment has been derived by Timoshenko.* This equation may be written in the following form:

$$(M_o)^2_{cr} = \left(\frac{\pi^2 B_y}{L^2} \right) \left(C_T + \frac{\pi^2 C_w}{L^2} \right) \quad \ldots . (2)$$

---

*The derivation is shown in Chapter V of Ref. 10. Timoshenko's derivation was made specifically for elastic buckling. However, the process can be extended to include also inelastic buckling if the stiffnesses are in the general terms of B_y, C_T, C_w instead of the usual elastic expressions EI_y, GK_T and EI_ω

where

$(M_o)_{cr}$ = End moment at initiation of buckling

B_y = Bending stiffness about the y-axis

L = Length of the beam

C_T = St. Venant torsional stiffness

C_w = Warping stiffness.

Equation 2 is the characteristic value of the differential equations of lateral buckling under pure moment for the following simply supported end conditions:

$$u = \frac{d^2u}{dz^2} = \beta = \frac{d^2\beta}{dz^2} = 0 \qquad \text{at } z = 0 \text{ and } z = L$$

The coordinate z is measured from one end of the beam along the deformed centroidal axis (see inset in Fig. 1).

The stiffness coefficients B_y, C_T and C_w are equal to the following expressions in the elastic range:

$$B_y = EI_y; \quad C_T = GK_T; \quad C_w = EI_\omega = \frac{EI_y d^2}{4} \qquad \text{.....(3)}$$

where I_y = Moment of inertia of the wide-flange section about its y-axis

K_T = St. Venant torsion constant[11]

I_ω = Warping constant[11]

d = Depth of the section (See Fig. 3).

If buckling takes place after certain portions of the cross section have already yielded, the expressions of Eq. 3 for the stiffnesses need not hold true. Yielding reduces the stiffness of a member, and therefore the inelastic values of B_y, C_T, and C_w will not remain constant. They will vary with the amount of yielding. The primary purpose of this report is to establish the variations of the stiffnesses due to yielding, and then to solve Eq. 2 for the values of the critical moments in the inelastic range.

The derivation of Eq. 2 implicity assumes the following two conditions: (1) The stiffnesses may not vary along the length of the member, and (2) the shear center must lie in the plane of bending (that is, the y-y plane). Since the moment is uniform along the whole length of the beam, each cross section is subjected to the same forces, and thus each cross section is yielded identically. Therefore the stiffnesses do not vary along the z-axis. Furthermore, yielding will be symmetrical about the y-y axis because of the symmetrical residual stress pattern (see Fig. 5). As a consequence, the shear center will remain on the y-y axis. Thus both conditions imposed by Eq. 2 are fulfilled for a yielded wide-flange beam.

II.3 DETERMINATION OF THE ZONES OF YIELDING

In order to be able to compute the stiffnesses governing the buckling equation in the inelastic range, the yielded pattern corresponding to the applied bending moment must be known. The relationships between the bending moment and the corresponding curvature and the yielded zones are derived in Appendix A by a step-by-step procedure, starting from the unloaded state and leading to successively more and more severe cases of yielding. The process consists of finding the curvature and the bending moment caused by given stress patterns. These stress-patterns (shown in Figs. 6 to 11), as well as the yielded configurations, are dependent on the cross sectional geometry (Fig. 3) and on the initial residual stress distribution (Fig. 5).

The equations expressing the relation between the moment M, the curvature ϕ, the compression flange yielding parameter α (Figs. 7 and 8) and the tension flange yielding parameter ψ (Figs. 9 and 10) are tabulated at the end of Appendix A. Several sample derivations are given at the beginning of this appendix to illustrate how the equations are developed from the equilibrium conditions.

The results of the computations are shown in Fig. 12 for the 8WF31 section. The curves in the upper portion of this figure show the variation of the moment and the curvature with compression flange yielding α, whereas the curves in the lower half of Fig. 12 give the relationship between M, ϕ, and the tension flange yielding parameter ψ.

With the aid of Fig. 12 it is thus possible to determine the extent of yielding corresponding to any moment. (See inset in Fig. 12.)*

II.4 STIFFNESSES OF THE YIELDED CROSS SECTION

In the previous section it was shown how the yield-pattern of a wide-flange cross section corresponding to a given moment can be obtained.

---

* Web yielding νd can be determined from equations given in Appendix A. Since the web contributes little to the lateral stiffness of the cross section, no M vs ν curves are shown.

The yielded configuration of the section is shown in the inset of Fig. 12. From this sketch it may be observed that yielding (cross-hatched area) is symmetrical about the y-y axis, and that the interface between the elastic and the plastic portions of the flange is inclined across the flange thickness. In order to simplify subsequent calculations this inclination is neglected; the simpler yield pattern is shown in Fig. 13. The compression flange is assumed yielded uniformly a distance αb from the toes of the flange, and the tension flange is yielded a distance ψb from the center. Since this simplification reduces the elastic core by a small amount, the foregoing assumption is conservative.

In the derivations of Appendix A it was stipulated that the stresses may nowhere exceed the yield stress σ_y.* As a consequence the strains in the plastic sections lie on the flat portion of the stress-strain diagram, where the modulus of elasticity is equal to zero. Since the bending stiffness B_y and the warping stiffness C_w are dependent on the modulus of elasticity (Eq. 3), only the elastic core can be assumed to furnish those stiffnesses. It has been shown[5] that at the start of lateral buckling St. Venant's torsional stiffness C_T is not dependent on the amount of yielding, and therefore the full elastic value of $C_T = GK_T$ can be used for substitution in the lateral buckling equation. Thus only the stiffnesses B_y and C_w need be computed for the unyielded core of the wide-flange cross section.

---

* A proof that this assumption is correct can be seen from Fig. 12, where the maximum curvature when both flanges are fully yielded is equal to $1.52\ \phi_y$. This curvature is considerably below the curvature at the start of strain hardening ($\phi_{st} \cong 12\ \phi_y$[3]), and thus the yielded portions can be assumed to have no resistance to additional bending.

Bending Stiffness B_y.

The bending stiffness of the elastic core about the y axis is equal to (See Fig. 13):

$$B_y = E \left[\frac{t}{12} (b-2\alpha b)^3 + \frac{tb^3}{12} - \frac{t}{12} (2\psi b)^3 \right]$$

A rearrangement of this expresssion yields the following equation for B_y:

$$B_y = EI_y B_1 \qquad \ldots\ldots(4)$$

where I_y is the moment of inertia of the original unyielded section, ($I_y = \frac{b^3 t}{6}$), and B_1 is a reduction factor which is equal to

$$B_1 = \frac{1}{2} \left[1 + (1-2\alpha)^3 - 8\psi^3 \right] \qquad \ldots\ldots(5)$$

This relationship between α, ψ and B_1 is illustrated in Fig. 14. When the section is fully elastic ($\alpha = \psi = 0$), $B_1 = 1.0$, and when $\alpha = \psi = 0.5$ (full yielding of the flanges), $B_1 = 0$.

Warping Stiffness C_w.

The warping stiffness of a section with unequal flanges has been determined (Eq. 231, Ref. 1) as

$$C_w = (E)\ (d-t)^2 \left[\frac{I_1\ I_2}{I_1+I_2} \right] \qquad \ldots\ldots(6)$$

where I_1 is the moment of inertia of the compression flange about the y-axis, and I_2 is the corresponding property of the tension flange. From Fig. 13 it is seen that

$$I_1 = \frac{b^3 t}{12} (1-2\alpha)^3 \qquad \text{. . . . .(7)}$$

$$I_2 = \frac{b^3 t}{12} (1-8\psi^3) \qquad \text{. . . . .(8)}$$

Substitution of Eqs. 7 and 8 into Eq. 6 gives the following expression for the warping rigidity:

$$C_w = EI_y \, (d-t)^2 \, B_2 \qquad \text{. . . . .(9)}$$

where I_y is the moment of inertia of the original section, and B_2 is a reduction factor equal to

$$B_2 = \frac{(1-8\psi^3)(1-2\alpha)^3}{4 \, B_1} \qquad \text{. . . . .(10)}$$

The curves relating α, ψ and B_2 are shown in Fig. 15. At $\alpha = \psi = 0$, $B_2 = 0.25$, thus fulfilling the fully elastic boundary condition. At $\alpha = 0.5$, that is when the compression flange is fully yielded, $B_2 = 0$ for any value of ψ. This means that when the effective section is a T-section, the warping rigidity is zero.(1)

The curves in Figs. 14 and 15 permit the determination of the stiffnesses B_y and C_w when α and ψ are known. In subsequent calculations it is desirable to have a direct relationship between the moment and the stiffness coefficients B_1 and B_2. This may be accomplished by eliminating α and ψ with the aid of Fig. 12, where the moment versus α and ψ curves are shown. The resulting curves for the 8WF31 section are given in Fig. 16, where moment is plotted directly against B_1 and B_2. Thus if M is known, the corresponding stiffnesses B_y and C_w can be immediately determined from this figure and from Eqs. 4 and 9.

II.5 THE INELASTIC BUCKLING CURVE.

The equation of buckling (Eq. 2) can be rearranged in the following manner:

$$(M_o)^2_{cr} L^4 - \pi^2 B_y C_T L^2 - \pi^4 C_w B_y = 0$$

If this equation is divided by $M_p^2 = Z^2 \sigma_y^2$ (where Z is the plastic modulus) and by r_y^4 (where r_y is the weak axis radius of gyration of the original cross section), and if the expressions for B_y, C_T and C_w are substituted from Eqs. 4, 3c and 9, the buckling equation can be written in the following non-dimensional form:

$$\left[\left(\frac{M_o}{M_p}\right)^2_{cr}\right]\left(\frac{L}{r_y}\right)^4 - \left[\left(\frac{\pi^2 EG}{\sigma_y^2}\right)\left(\frac{AK_T}{Z^2}\right) B_1\right]\left(\frac{L}{r_y}\right)^2 -$$

$$- \left[\left(\frac{\pi^2 E}{\sigma_y}\right)^2 \frac{A^2(d-t)^2}{Z^2} (B_1 B_2)\right] = 0 \qquad \ldots\ldots(11)$$

Equation 11 is a fourth order equation in that slenderness ratio L/r_y which corresponds to the critical moment at which lateral buckling commences. The coefficients of L/r_y consist of the cross sectional constants $\frac{AK_T}{Z^2}$ and $\frac{A^2(d-t)^2}{Z^2}$ (where A is the cross sectional area of the original section), the material constants $\frac{\pi^2 EG}{\sigma_y^2}$ and $(\frac{\pi^2 E}{\sigma_y})^2$, the non-dimensional bending moment M_o/M_p, and the coefficients B_1 and B_2 which are directly dependent on the moment.

The construction of the critical length-versus-moment curve of Fig. 1 can be performed in the following manner: For a given wide-flange cross section first the moment versus B_1 and B_2 curves are developed (as shown in Fig. 16 for the 8WF31 section). Next, Eq. 11 is solved for L/r_y for assumed values of the moment. This is done for a sufficient number of moment values until the whole course of the buckling curve is established. Figure 17 shows such a curve for the 8WF31 section. For moments from 0 to 0.631 M_p elastic buckling governs. In this region the stiffnesses B_y and C_w are undiminished. For a moment larger than 0.631 M_p, yielding takes place due to the presence of residual stresses before the section buckles. Points on this portion of the curve are computed by assuming a moment ($M_o > 0.63\ M_p$), finding the values of B_1 and B_2 corresponding to this moment from Fig. 16, and solving Eq. 11 for the critical weak axis slenderness ratio. The increments of moment used for the inelastic part of the curve in Fig. 17 were chosen at 0.05 M_p.

The cut-off point for the start of strain hardening (at $L/r_y = 20$ in Fig. 17) is computed by a method suggested in Ref. 3. Equation 2 is solved by setting $B_y = E_{st}I_y$, $C_T = G_{st}K_T$ and $C_w = \frac{E_{st}I_y d^2}{4}$, where

E_{st} and G_{st} are strain hardening moduli. It has been shown(20) that this point, at which the whole section can be assumed to be strain hardened at buckling, occurs at a slenderness ratio of about 20 for all rolled wide-flange sections.

The curve in Fig. 17 describes the buckling behavior of an 8WF31 section over its whole length range. Inelastic buckling governs up to a length of about 220 r_y, or to about 37 feet. Thus it can be seen that for practical lengths one must consider the reduction in buckling strength due to yielding.

The error involved in assuming that yielding does not start until the yield moment $M_y = S\,\sigma_y$ (where S is the section modulus) is reached is illustrated in Fig. 18. In this figure curve A represents the inelastic solution including residual stresses, and curve B is a continuation of the elastic Euler hyperbola until $(M_o)_{cr} = M_y$. A straight line transition has been used from the yield moment to $(M_o)_{cr} = M_p$ at the start of strain hardening. It can be seen that the residual stresses have a considerable influence on the buckling strength, and that their neglect may lead to results which may be as much as 30% unconservative.

The usual design procedure which does not permit the use of moments larger than the yield moment is shown by the dashed horizontal line in Fig. 18. One can note that for $L/r_y > 90$ this rule leads to unconservative answers, whereas in the range of $0 < L/r_y < 90$ the full strength of the beam is not utilized.

III. SIMPLIFICATION OF THE PROCEDURE

A method has been presented for the determination of the buckling curves for wide-flange beams failing by inelastic lateral buckling. Numerical results are shown for the 8WF31 section in Fig. 16. Additional calculations by the same procedure were made for the 27WF96, the 14WF142 and the 14WF246 section. The results of the calculations are shown as the solid line curves in Fig. 19.

This method of computing the inelastic lateral buckling strength has one serious shortcoming: the computational work is too laborious. The main reason for this is the complex geometry of the stress patterns resulting from the cross sectional shape of the wide-flange section and the residual stress existing before load application.

A simplification of the calculations may be achieved as follows: In Fig. 20 are shown the reduction curves for the four sections for which computations were made (27WF94, 8WF31, 14WF142, 14WF246). In the upper portion of the figure the M/M_p versus B_1 relationship is given, while in the lower half the curves for M/M_p versus B_2 are shown. It can be observed from this figure that for even these geometrically dissimilar wide-flange sections the range in which these curves lie is not very great. Therefore no great error will result if one average curve is used for any wide-flange section. These approximate average curves are shown as heavy solid lines in Fig. 20.

The use of these average curves for B_1 and B_2 simplify the calculations considerably. All that is necessary for the determination of the buckling curve is the solution of Eq. 11 for $(L/r_y)_{cr}$ for the assumed moment values $(M_o/M_p)_{cr}$ using B_1 and B_2 from the average curves in Fig.20.

The lateral buckling equation (Eq. 11) can be written in the following form:

$$\left[\left(\frac{M_o}{M_p}\right)_{cr}^2\right]\left(\frac{L}{r_y}\right)^4 - \left[\left(\frac{\pi^2 EG}{\sigma_y^2}\right)\left(\frac{Ad}{Z}\right)^2\left(\frac{K_T}{Ad^2}\right)(B_1)\right]\left(\frac{L}{r_y}\right)^2 -$$

$$-\left[\left(\frac{\pi^2 E}{\sigma_y}\right)^2\left(\frac{Ad}{Z}\right)^2\left(1-\frac{t}{d}\right)^2(B_1B_2)\right] = 0 \qquad \ldots\ldots(12)$$

In this equation the coefficients $\frac{\pi^2 EG}{\sigma_y^2}$ and $\left(\frac{\pi^2 E}{\sigma_y}\right)^2$ are constants, depending on the properties of the material. Furthermore, a computation of (Ad/Z) and (1-t/d) for a majority of the tabulated wide-flange sections has shown that these coefficients are nearly constant for all sections. The average values of these constants are $\frac{Ad}{Z} \cong 2.53$ and $(1-t/d) \cong 0.950$. Substitution of the material constants of $\sigma_y = 33$ ksi, $E = 30{,}000$ ksi and $G = 11{,}500$ ksi, and the average cross sectional constants $\frac{Ad}{Z}$ and 1-t/d into Eq. 12 leads to the following explicit equation for the critical length:

$$\left(\frac{L}{r_y}\right)_{cr} = \sqrt{\frac{10\ D_T B_1}{(M_o/M_p)_{cr}^2}\left[1+\sqrt{1+\frac{4.65\times 10^6 (B_2/B_1)(M_o/M_p)^2}{D_T^2}}\ \right]} \qquad \ldots\ldots(13)$$

where the coefficient D_T is equal to

$$D_T = \frac{K_T \times 10^6}{Ad^2} \qquad \text{. . . . .(14)}$$

An examination of Eq. 13 shows that the critical length corresponding to a given moment is dependent only on the non-dimensional ratio D_T. Values of this coefficient are tabulated in a table in Appendix B. The values of D_T for sections usually used as beams vary from about 200 to 900. Since D_T = 219 for the 27WF94 section, and D_T = 925 for the 8WF31 section, the curves for the beams fall into the narrow band between the curves for the 8WF31 and the 27WF94 sections in Fig. 19.

The buckling curves resulting from using the above simplifications are shown as dashed lines in Fig. 19 for the 8WF31 and the 27WF94 sections. The difference between the "exact" curves and the approximate curves is quite negligible, especially in the inelastic range. It may therefore be concluded that the approximations do not greatly influence the final result, and thus a relatively simple way has been found to determine inelastic buckling curves for as-rolled wide-flange sections.

IV. COMPARISON WITH DESIGN APPROXIMATIONS

The fact that the buckling strength of beams is reduced due to yielding before the theoretical yield moment M_y is reached has been known for some time.[12] Because no direct computation of the reduction has been available, empirical design approximations have been suggested for the computation of the critical moment in the inelastic range. These approximations can be grouped into two categories: One of these methods is to provide an empirically determined transition curve between the elastic Euler hyperbola and an allowable maximum moment at zero length. The other method consists of computing the critical moment by the elastic formulas, and then to reduce this "ideal" moment in accordance with an empirically determined reduction curve to an "allowable" moment. The first approach has been used extensively in this country[12], and the latter is the basis of the German buckling specifications.[13]

In the following one of each of the above discussed procedures will be compared with the "exact" theory of this report.

IV.1 COMPARISON WITH A TRANSITION CURVE METHOD

It has been shown[12] that the critical elastic allowable lateral buckling stress can be expressed by the following approximate equation:

$$(\sigma_{cr})_w = \frac{12 \times 10^6}{\frac{Ld}{bt}} \qquad \ldots\ldots(15)$$

where $(\sigma_{cr})_w$ is the critical working stress (psi). The terms L, d, b and t are as defined in Fig. 1 and 3. The maximum value of $(\sigma_{cr})_w$ is the yield stress σ_y divided by a safety factor. If the minimum yield stress is specified as $\sigma_y = 33$ ksi and if the maximum allowable stress is 20 ksi[14], the safety factor is 1.65. The critical stress in Eq. 15 can thus be written in terms of the ultimate stress as

$$(\sigma_{cr})_u = S.F. \times (\sigma_{cr})_w = \frac{12 \times 10^6 \times 1.65}{Ld/bt} = \frac{19.8 \times 10^6}{Ld/bt}$$

Multiplying the critical stress by the section modulus S and non-dimensionalizing it through division by $M_p = Z\,\sigma_y$, the following expression results for the critical moment:

$$\left(\frac{M_o}{M_p}\right)_{cr} = \frac{1}{f}\left(\frac{600}{Ld/bt}\right) \quad \ldots\ldots(16)$$

where f is the shape-factor. Equation 16 is a non-dimensional form of the AISC lateral buckling rule.[14] A plot of this equation is shown as a heavy solid curve in Fig. 21. Since the limiting moment of Eq. 16 is the yield moment M_y, the curve is cut-off by a horizontal plateau at $M_o = 0.876\ M_p$ (if an average value of $f = 1.14$ is used as the shape factor) and at $Ld/bt = 600$. On the same figure (Fig. 21) are also plotted the "exact" curves computed in this report for four sections. It may be observed that the AISC rule is conservative in the ranges of $0 < \frac{Ld}{bt} < 400$ and above about $Ld/bt = 800$. In the range $400 < \frac{Ld}{bt} < 800$ the rule results in a reduction of the safety factor below the minimum value of 1.65.

In order to keep the safety factor everywhere above 1.65, the following transition curve has been proposed[12]:

$$\sigma_{cr} = 33{,}000 - 0.0125 \quad (Ld/bt)^2 \qquad \ldots\ldots(17)$$

Equation 17 can be non-dimensionalized into

$$\left(\frac{M_o}{M_p}\right)_{cr} = \frac{1}{f}\left[1 - 0.378 \times 10^6 \ (Ld/bt)^2\right] \qquad \ldots\ldots(18)$$

This transition curve is shown as a dashed curve in Fig. 21. It lies everywhere below the theoretically determined curves, and is thus conservative. It's range of application is $0 < \frac{Ld}{bt} < 775$.

A possible new design approach, which would retain the well known Ld/bt parameter and which would make more efficient use of the inelastic strength of the beam, is shown in Fig. 22. A straight line transition curve between elastic buckling ($Ld/bt \gg 800$) and buckling in the strain hardening range is shown in this figure. The corresponding equations are as follows:

$$\left(\frac{M_o}{M_p}\right)_{cr} = 1.00 \qquad \ldots\ldots(21)$$

$$\text{for } 0 \leqslant \frac{Ld}{bt} \leqslant 35 \ \frac{r_y d}{bt}$$

$$\left(\frac{M_o}{M_p}\right)_{cr} = 1.000 - \frac{0.342\left[\frac{Ld}{bt} - 35\ \frac{r_y d}{bt}\right]}{800 - 35\ \frac{r_y d}{bt}} \qquad \ldots\ldots(22)$$

. . . . . (22)

$$\text{for}\quad 35\ \frac{r_y d}{bt} \leqslant \frac{Ld}{bt} \leqslant 800$$

$$\left(\frac{M_o}{M_p}\right)_{cr} = \frac{526}{Ld/bt} \qquad \ldots\ldots(23)$$

$$\text{for}\quad 800 \leqslant \frac{Ld}{bt} \leqslant \infty$$

Equation 21 represents the lateral bracing spacing rule used in plastic design(18), which states that in the vicinity of a plastic hinge (that is $M_o = M_p$), the critical length for uniform moment is equal to 35 r_y.* (Since the non-dimensional length parameter used is Ld/bt, the slenderness ratio $\frac{L}{r_y} = \frac{Ld}{bt} \times \frac{bt}{dr_y}$). Equation 23 is the AISC Ld/bt rule, which governs elastic instability (see Eq. 16, where the shape factor is set equal to 1.14). Equation 22 represents the straight line transition between the end points of Eq. 21 and 23. In Fig. 22 the curves of these three equations are compared with the "exact" solutions for four cross sections. It is seen that the proposed curves utilize the inelastic strength of the beam, while at the same time they represent a safe lower bound.

---

* This rule has been shown to be correct by theoretical and experimental means.(3)(19)

IV.2 COMPARISON WITH A REDUCTION CURVE METHOD

The Column Research Council[15] has proposed that for an approximate determination of the inelastic buckling strength of beams it can be assumed that the relationship between elastic and inelastic buckling strength is the same for beams as for columns.* Since the inelastic buckling strength of axially loaded columns is well known,[15] the relationship between elastic (Euler) buckling and plastic (Engesser-Shanley) buckling can be easily established. The elastic, or "ideal" buckling stress of a column is $\sigma_{cr} = \frac{\pi^2 EI}{L^2}$. If this expression is divided by σ_y, and the values of $\sigma_y = 33$ ksi and $E = 30,000$ ksi are substituted, the following equation results for the ideal stress:

$$\left(\frac{\sigma_{cr}}{\sigma_y}\right)_i = \frac{8970}{(L/r)^2} \quad \text{.....(19)}$$

The inelastic buckling stress for wide-flange sections can be approximated by[17]

$$\left(\frac{\sigma_{cr}}{\sigma_y}\right)_{all} = 1 - \frac{(L/r)}{645} - \frac{(L/r)^2}{111,000} \quad \text{.....(20)}$$

The curve showing the ideal-versus-allowable stress relationship, as computed by eliminating the slenderness ratio from Eqs. 19 and 20 is shown in Fig. 23. Since it is assumed that the same curve will approximate lateral buckling, the coordinates in this figure are expressed as critical bending moments.

---

* This same philosophy underlies the German buckling specifications.[14] See also Ref. 16 for further explanation of this method.

The lateral buckling strengths of a beam can be thus approximated by calculating the elastic critical moment (by keeping $B_1 = 1.0$ and $B_2 = 0.25$ in Eq. 11), and then entering the reduction curve of Fig. 22 and directly reading off the inelastic "allowable" moment.* The results of the computations for the 8WF31 section are shown in Fig. 24, where the approximate curve is drawn as a dashed line. The comparison is fair, with a maximum deviation being about 5%.

---

* This method is especially useful for cases where the end conditions of the beam are not simple and where the beam is subjected to lateral loads or a moment gradient. Elastic solutions are available for these cases(16), whereas the computation of "exact" inelastic solutions seems too difficult at this time.

V. CONCLUSIONS

In this report a method has been presented for the determination of the inelastic buckling strength of steel wide-flange beams failing by lateral buckling. The method has been illustrated for the case of wide-flange beams because of their frequent occurrence in civil engineering structures. The type of solution, however, may be adapted for any cross sectional shape under any residual stress distribution, provided that bending takes place in a plane of symmetry, and that the residual stresses are also symmetrical about the plane of bending. A further stipulation is that bending is uniform and that the stress-strain diagram can be approximated by straight lines.

An extension of this work would be to compute the lateral buckling strength of beams subjected to unequal bending moments or to loads placed between the supports. In this case the moment, and thus the distribution of yielding along the length of the beam, is non-uniform. The best way of obtaining a solution would be to solve the differential equations of lateral buckling by the method of finite differences, possibly with the aid of a digital computer. The stiffness reduction curves of Fig. 20 can be utilized in these calculations.

The critical length versus end moment curves for a given wide-flange section are obtained in the following manner:

(1) The yielded zones corresponding to a given inelastic moment are determined with the aid of the conditions of equilibrium. General equations are given in Appendix A, and the curves

relating compression flange and tension flange yielding corresponding to various moments are shown in Fig. 12 for the 8WF31 shape.

(2) The weak axis bending stiffness B_y and the warping stiffness C_w for the "effective" reduced section are computed by Eqs.4 and 5 and Eqs. 9 and 10, respectively. Curves showing the reduction coefficients B_1 and B_2 are shown in Fig. 16 for the 8WF31 section. The St. Venant's torsional stiffness is not reduced due to yielding.[5]

(3) The lateral buckling equation (Eq. 11) is solved for the critical length for various assumed values of the inelastic moment and the corresponding reduced stiffness. The resulting curve for the 8WF31 section is shown in Fig. 17.

A simplification of this procedure can be accomplished by noting that the moment versus stiffness reduction coefficients B_1 and B_2 are nearly the same for all wide-flange sections, (see Fig. 20) and that certain non-dimensional cross sectional properties can be assumed to vary only a small amount for the tabulated rolled wide-flange shapes. The critical length corresponding to any inelastic moment can be expressed by Eq. 13.

The results of the "exact" procedures have been compared with currently used design approximations (see Figs. 21 and 24), for the determination of inelastic buckling strength. It was shown that the AISC Ld/bt rule, coupled with a parabolic transition curve in the inelastic range, provides a suitable lower bound for wide-flange sections.

A possible modification of this rule is illustrated in Fig. 22. The corresponding design equations are Eqs. 21, 22 and 23. This modified rule would make better use of the inelastic strength of beams, especially for lengths below $\frac{Ld}{bt} = 300$.

VI. A C K N O W L E D G E M E N T S

This study is part of the general investigation "Welded Continuous Frames and Their Components" currently being carried out at the Fritz Engineering Laboratory of the Civil Engineering Department of Lehigh University under the general direction of Lynn S. Beedle. The investigation is sponsored jointly by the Welding Research Council and the Department of the Navy, with funds furnished by the American Iron and Steel Institute, American Institute of Steel Construction, Office of Naval Research, Bureau of Ships and Bureau of Yards and Docks.

The author expresses his thanks to Robert L. Ketter and Tadao Kusuda for their helpful suggestions.

VII. NOMENCLATURE

A = Cross sectional area (in.^{2})

B_1, B_2 = Stiffness reduction coefficients

B_y = Weak axis bending stiffness (lb.-in.^{2})

C_T = St. Venant torsional stiffness (lb.-in.^{2})

C_w = Warping stiffness (lb.-in.^{4})

D_T = Cross sectional coefficient defined by Eq. 14

E = Modulus of elasticity (psi)

E_{st} = Strain hardening modulus (psi)

G = Shear modulus (psi)

G_{st} = Shear modulus in the strain hardening range (psi)

I_y = Moment of inertia about the y-y axis (in.^{4})

I_1, I_2 = Effective moments of inertia of the compression flange and the tension flange, respectively. (in.^{4})

I_w = Warping coefficient (in.^{6})

K_T = Torsion coefficient (in.^{4})

L = Unsupported length of the beam (in.)

L_{cr} = Critical length (in.)

M_o = Applied end bending moment (in.-lbs.)

M_m = Ultimate moment, (in.-lbs.)

$(M_o)_{cr}$ = Critical end moment (in.-lbs.)

M_p = Plastic moment (in.-lbs.)

M_y = Yield moment (in.-lbs.)

S = Section modulus (in.^{3})

Z = Plastic modulus (in.^{3})

T, U, W = Non-dimensional coefficients defined by Eqs. A-8, A-13 and A-11, respectively

b = Width of flange (in.)

d = Depth of beam (in.)

f = Shape factor

r_y = Weak axis radius of gyration (in.)

t = Thickness of flange (in.)

u = Lateral deflection (in.)

v = Transverse deflection (in.)

w = Thickness of web (in.)

αb = Compression flange yielding (in.)

β = Angle of twist

ϕ, ϕ_y, ϕ_{st} = Curvature, curvature at the yield point, curvature at the onset of strain hardening, respectively.

ψb = Tension flange yielding (in.)

νd, τd = Web yielding (in.)

σ_{MT}, σ_{MB} = Compression and tension flange stresses, respectively (psi)

σ_y = Yield stress (psi)

σ_{rc}, σ_{rt} = Maximum compressive and tensile residual stresses, respectively (psi)

σ_{cr} = Critical stress (psi)

APPENDIX A

The relationship between the applied bending moment and the resulting curvature and yield patterns are developed below by a step-by-step procedure.

a) The Unloaded State

In the unloaded state only the residual stresses are present on the cross section. Their magnitude and distribution is shown in Fig. 5.

b) Elastic Behavior

Figure 6 shows the stresses on the three components of the cross section (the compression flange, the web, and the tension flange). In this figure σ_{MT} and σ_{MB} are the absolute values of the maximum top or compression flange stress and the bottom or tension flange stress, respectively. The angle ϕ is the curvature of the section in the plane of the web. Strains are assumed proportional to the distance from the neutral axis.

If the forces in each of these parts due to the stresses are summed and equated to zero, it is found that

$$\sigma_{MT} = \sigma_{MB} \tag{A-1}$$

The summation of the moments about the center of the section due to the assumed stress distribution gives

$$M = \sigma_{MT} S \tag{A-2}$$

where M is the moment applied to the section and S is the section modulus.

Because it will be more convenient to work with non-dimensional ratios, both sides of equation A-2 will be divided by $M_p = \sigma_y Z$, where

M_p is the fully plastic moment, and Z is the plastic modulus. Thus, the non-dimensional form of Eq. A-2 is

$$\frac{M}{M_p} = \frac{\sigma_{MT} S}{\sigma_y Z} = \frac{1}{f} \frac{\sigma_{MT}}{\sigma_y} \tag{A-3}$$

where f = Z/S is the shape factor of the cross section.

The curvature ϕ is obtained by geometry from Fig. 6.

$$\tan E\phi \cong E\phi = \frac{\sigma_{MT} + \sigma_{MB}}{d} = \frac{2\,\sigma_{MT}}{d} \tag{A-4}$$

If the yield stress σ_y is used in Eq. A-4, the "initial yield curvature" $E\phi_y$ is obtained. Therefore

$$E\phi_y = \frac{2\,\sigma_y}{d} \tag{A-5}$$

and

$$\frac{\phi}{\phi_y} = \frac{\sigma_{MT}}{\sigma_y} \tag{A-6}$$

The limit of elastic behavior is reached when $\sigma_{MT} + \sigma_{rc} = \sigma_y$ or $\sigma_{MB} + \sigma_{rt} = \sigma_y$, whichever occurs first. Since $\sigma_{MT} = \sigma_{MB}$ in the elastic range, and $\sigma_{rc} > \sigma_{rt}$ (see Eq. 1), yielding will first commence in the compression flange. Thus

$$\left(\frac{\sigma_{MT}}{\sigma_y}\right)_{el.lim.} = 1 - \frac{\sigma_{rc}}{\sigma_y} \tag{A-7}$$

Using the abbreviation

$$T = 1 - \frac{\sigma_{rc}}{\sigma_y} \tag{A-8}$$

the values of the moment and the curvature at the commencement of yielding are:

$$\left(\frac{M}{M_p}\right)_{el.lim} = \frac{T}{f} \text{ and } \left(\frac{\phi}{\phi_y}\right)_{el.lim} = T \tag{A-9}$$

c) Part of the Cross Section is Yielded

From Fig. 6 it can be seen that the yield stress will first be reached at the tips of the compression flange, since it is here that the maximum compressive stresses due to bending moment and the maximum compressive residual stress are additive. The various stages of this partially yielded condition are shown in Figs. 7 to 11 for the three components of the cross section. Figures 7 and 8 show the compression flange. Figure 7 gives the case where yielding has not yet penetrated through the thickness of the flange and Fig. 8 shows the case where yielding has penetrated through the flange. Figures 9 and 10 give the corresponding situation on the lower flange, while Fig. 11 depicts the stresses in the web.

Yielding commences first on the outside faces of the tips of the compression flange, and it progresses toward the center of the flange. The amount of yielding measured from the outside face of the flange is αb. The maximum extent of possible yielding is when yielding has progressed over the whole width of this face; thus $(\alpha b)_{max} = \frac{b}{2}$ or $0 \leqslant \alpha \leqslant \frac{1}{2}$. The tension flange (Fig. 9) will begin to yield at the center of the flange, and yielding will progress toward the tips. The amount of yielding in this flange is designated as ψb (see Figs. 9 and 10) and therefore $0 \leqslant \psi \leqslant \frac{1}{2}$.

From Figs. 7 and 8 the following relationship can be developed for the stress σ_{MT}:

$$\sigma_{rc} + \sigma_{MT} = \sigma_y + 2\alpha\,(\sigma_{rc} + \sigma_{rt})$$

In non-dimensional form

$$\frac{\sigma_{MT}}{\sigma_y} = 1 - \frac{\sigma_{rc}}{\sigma_y} + 2\,\alpha\left(\frac{\sigma_{rc} + \sigma_{rt}}{\sigma_y}\right) = T - 2\alpha W \qquad \text{(A-10)}$$

where

$$W = \frac{\sigma_{rc} + \sigma_{rt}}{\sigma_y} \qquad \text{(A-11)}$$

By similar considerations from Figs. 9 or 10, the bottom flange stress is:

$$\frac{\sigma_{MB}}{\sigma_y} = 1 - \frac{\sigma_{rt}}{\sigma_y} + 2\psi\left(\frac{\sigma_{rc} + \sigma_{rt}}{\sigma_y}\right) = U + 2\psi W \qquad \text{(A-12)}$$

where

$$U = 1 - \frac{\sigma_{rt}}{\sigma_y} \qquad \text{(A-13)}$$

The relationship between top flange and bottom flange stresses (From Figs. 6 or 11) is determined by the geometry of similar triangles:

$$\frac{\sigma_{MT} + \sigma_{MB}}{d} = \frac{\sigma_{MB} + \sigma_{rt}}{d - \frac{\sigma_{MT}}{E\phi} + \frac{\sigma_{rt}}{E\phi}}$$

Non-dimensionalizing this expression, and solving for σ_{MB},

$$\frac{\sigma_{MB}}{\sigma_y} = 2\frac{\phi}{\phi_y} - \frac{\sigma_{MT}}{\sigma_y} \qquad \text{(A-14)}$$

<u>d) Compression Flange Partially Yielded, $tE\phi > 2\alpha(\sigma_{rc} + \sigma_{rt})$, Tension Flange and Web Still Elastic</u>

The stress picture at the initiation of yielding is shown in Fig. 7 for the top flange. The tension flange and the web remain elastic, and the stresses for these components are shown in Fig. 6.

Summing up forces on the cross section:

$$\Sigma P = 0 = (\sigma_{MT} - \frac{1}{2}tE\phi)bt - \frac{\alpha b}{3}\left[\frac{4\alpha^2(\sigma_{rc} + \sigma_{rt})^2}{E\phi}\right]^2 + \qquad \text{Top Flange}$$

$$+ W(d-2t)\left[(\sigma_{MT} - tE\phi) - \frac{1}{2}(\sigma_{MB} + \sigma_{MT} - 2tE\phi)\right] - \qquad \text{Web}$$

$$- (\sigma_{MB} - \frac{1}{2}tE\phi)\,bt \qquad \text{Bottom Flange}$$

If the expression above is divided by σ_y, and if the values of ϕ_y (Eq. A-5), σ_{MT} (Eq. A-10) and σ_{MB} (Eq. A-14) are substituted, the following non-dimensional equation is obtained for the curvature:

$$(\phi/\phi_y)^2 - (T+2\alpha W)\ (\phi/\phi_y) + \frac{\alpha^3 W^2\ (d/t)}{3(1+\frac{Wd}{2bt} - \frac{W}{b})} = 0 \qquad \text{(A-15)}$$

Equation A-15 reduces to Eq. A-9 when $\alpha = 0$, that is, at the inception of yielding. The upper limit for Eq. A-15 is when the inside face of the compression flange commences to yield, or when yielding has progressed to the outside face of the tension flange, whichever occurs first.

The first of these limits, i.e., when the inside face begins to yield, occurs when $tE\phi = 2\alpha\ (\sigma_{rc} + \sigma_{rt})$ (See Fig. 7). In non-dimensional form

$$(\phi/\phi_y)_{(1)} = (d/t)\ W\alpha_{(1)} \qquad \text{(A-16)}$$

Substituting the value of $(\phi/\phi_y)_{(1)}$ from A-16 into Eq. A-15, the following quadratic equation is obtained for $\alpha_{(1)}$:

$$\alpha^2_{(1)} + 3(1+\frac{dw}{2bt} - \frac{w}{b})\left[(d/t-2)\,\alpha_{(1)} - \frac{T}{W}\right] = 0 \qquad \text{(A-17)}$$

The other alternative, that is, when the tension flange commences to yield before the top flange has yielded through its thickness, requires that $\sigma_{MB} = \sigma_y - \sigma_{rt}$. This relationship is solved for the curvature in non-dimensional form (using Eq. A-14) as

Hence $$\frac{\sigma_{MB}}{\sigma_y} = 1 - \frac{\sigma_{rt}}{\sigma_y} = 2\ \phi/\phi_y - 1 + \frac{\sigma_{rc}}{\sigma_y} - 2\alpha W$$

$$(\phi/\phi_y)_{(2)} = 1 - W\ (\ 1/2 - \alpha_{(2)}\ ) \tag{A-18}$$

Substituting this value of $(\phi/\phi_y)_{(2)}$ into Eq. A-15, the following equation is obtained for the value of $\alpha_{(2)}$:

$$\left[\frac{W^2(d/t)}{3(1+\frac{dw}{2bt}-\frac{w}{b}}\right]\alpha^3_{(2)} - W^2\alpha^2_{(2)} - TW\alpha_{(2)} +$$

$$+ (1-T) + W\ (\ \frac{W}{4} + \frac{T}{2} - 1) = 0 \tag{A-19}$$

The summation of moments about the centroid of the section yields the following non-dimensional expression for the bending moment.

$$\frac{M}{M_p} = (\phi/\phi_y)\ (S/Z) - \frac{\alpha^3 bd^2 W^2}{3Z\ \phi/\phi_y}\left[1 - \frac{\alpha\ W}{2\ \phi/\phi_y}\right] \tag{A-20}$$

The limits of Eq. A-20 are the same as the limits of the curvature equation, (Eq. A-15).

e) More Severe Cases of Yielding

The procedure which was outlined in the preceding sections is employed to obtain the curvature and the limits of the application of the equations for further yielding. In all cases the sum of the forces is equated to zero to obtain the curvature, and moments are taken about the centroid of the original cross section to obtain the bending moment. The resulting equations are summarized below:

1) The limit of elastic behavior (Fig. 6)

Moment: $(M/M_p)_{el.\ lim.} = T/f$

Curvature: $(\phi/\phi_y)_{el.\ lim.} = T$

2) Compression flange partially yielded (Fig. 7), tension flange and web elastic (Fig. 6)

Curvature:

$$(\phi/\phi_y)^2 - (T+2\alpha W)\ (\phi/\phi_y) + \frac{\alpha^3 W^2 (d/t)}{3(1+\frac{wd}{2bt} - \frac{w}{b})} = 0$$

Moment:

$$\frac{M}{M_p} = (\phi/\phi_y)\ (1/f) - \frac{\alpha^3 b d^2 W^2}{3Z\ (\phi/\phi_y)} \left[1 - \frac{\alpha W}{2\ \phi/\phi_y}\right]$$

Limits: $0 \leqslant \alpha \leqslant \alpha_{(1)}$ or $0 \leqslant \alpha \leqslant \alpha_{(2)}$ whichever is smaller;

$\alpha_{(1)}$ and $\alpha_{(2)}$ are defined by:

$$\alpha^2_{(1)} + 3\left[\frac{dw}{2bt} - \frac{w}{b} + 1\right]\left[(d/t - 2)\ \alpha_{(1)} - \frac{T}{W}\right] = 0$$

$$\left[\frac{W^2(d/t)}{3(\frac{dw}{2bt} - \frac{w}{b} + 1)}\right] \alpha^3_{(2)} - W^2 \alpha^2_{(2)} - TW\alpha_{(2)} + \left[1 - T + W\ (\frac{W}{4} + \frac{T}{2} - 1)\right] = 0$$

3) Compression flange partially yielded (Fig. 8), tension flange and web elastic (Fig. 7)

Curvature:

$$(\phi/\phi_y)^2 + \left\{ 3W(d/t) \left[d/t \left(1 + \frac{dw}{2bt} - \frac{w}{b} \right) - \alpha \right] \right\} (\phi/\phi_y) +$$

$$+ 3W(d/t)^2 \left\{ W\alpha^2 - \left(1 + \frac{dw}{2bt} - \frac{w}{b} \right) (T + 2\alpha W) \right\} = 0$$

Moment:

$$\frac{M}{M_p} = \left(\frac{\phi}{\phi_y}\right)\left(\frac{1}{f}\right) - \frac{btd}{Z} \left\{ \left(\frac{\phi}{\phi_y}\right)^2 \frac{(t/d)^2}{3W} \left(1 - \frac{3t}{d}\right) + \alpha^2 W(1-t/d) \right.$$

$$\left. - \alpha (t/d) \quad (\phi/\phi_y) \quad \left(1 - \frac{4t}{3d}\right) \right\}$$

Limits:

$$\alpha_{(1)} \leqslant \alpha \leqslant \alpha_{(3)} \; ; \qquad \psi = 0$$

where $\alpha_{(3)}$ is defined by:

$$\left\{ W^2 \left[1 + 3\,(d/t)\,(d/t-1) \right] \right\} \alpha^2_{(3)} -$$

$$- \left\{ W\left(3\frac{d}{t} - 2\right) + W^2 \left[1 + 3\,(d/t)^2 \left(1 + \frac{wd}{2bt} - \frac{w}{b}\right) - \frac{3}{2}\,\frac{d}{t} \right] \right\} \alpha_{(3)} +$$

$$+ \left\{ 1 - W + \frac{W^2}{4} + 3W\,(d/t)^2 \left(1 + \frac{wd}{2bt} - \frac{w}{b}\right) \left(1 - T - \frac{W}{2}\right) \right\} = 0$$

4) Compression flange partially yielded (Fig. 7), tension flange partially yielded (Fig. 9), web elastic (Fig. 6).

Curvature:

$$(\phi/\phi_y)^2 - (T + 2\alpha W) \quad (\phi/\phi_y) + \frac{W^2 (\alpha^3 - \psi^3)(d/t)}{3\left(1 + \frac{wd}{2bt} - \frac{w}{b}\right)} = 0$$

Moment:

$$\frac{M}{M_p} = \left(\frac{\emptyset}{\emptyset_y}\right)\left(\frac{1}{f}\right) - \frac{bd^2 W^2}{3Z\,(\emptyset/\emptyset_y)}\left[\alpha^3 + \psi^3 - \frac{W}{2\,(\emptyset/\emptyset_y)}\,(\alpha^4 + \psi^4)\right]$$

Limits:

$$\alpha_{(2)} \leqslant \alpha \leqslant \alpha_{(4)}; \quad 0 \leqslant \psi \leqslant \psi_{(4)}$$

where $\alpha_{(4)}$ and $\psi_{(4)}$ are defined by:

$$\psi_{(4)} = \alpha_{(4)}\,(d/t - 1) - \left(\frac{1}{W} - \frac{1}{2}\right);$$

$$\alpha^3_{(4)} - \left[\frac{3\left(\frac{d}{t} - 1\right)^2\left(\frac{1}{W} - \frac{1}{2}\right) + 3\left(\frac{d}{t} - 2\right)\left(1 + \frac{wd}{2bt} - \frac{w}{b}\right)}{(d/t - 1)^3 - 1}\right]\alpha^2_{(4)} +$$

$$+ \left[\frac{3(d/t - 1)\left(\frac{1}{2} - \frac{1}{W}\right)^2 + \frac{3T}{W}\left(1 + \frac{wd}{2bt} - \frac{w}{b}\right)}{(d/t - 1)^3 - 1}\right]\alpha_{(4)} - \frac{\frac{1}{W} - \frac{1}{2}}{(d/t-1)^3 - 1} = 0$$

The relationship between α, ψ and $\emptyset/\emptyset_y$ is:

$$\psi = \frac{1}{W}\left[\frac{\emptyset}{\emptyset_y} - 1\right] + \left[\frac{1}{2} - \alpha\right]$$

5) Compression flange partially yielded, (Fig. 8), tension flange partially yielded, (Fig. 9), web elastic, (Fig. 6).

Curvature:

$$\left(\frac{\emptyset}{\emptyset_y}\right)^3 + \left\{3\,W(d/t)\left[(d/t)\left(1 - \frac{w}{b}\right) + (d/t)^2\left(\frac{w}{2b}\right) - \alpha\right]\right\}\left(\frac{\emptyset}{\emptyset_y}\right)^2 +$$

$$+ \left\{3W\,(d/t)^2\left[W\alpha^2 - \left(1 + \frac{wd}{2bt} - \frac{w}{b}\right)(T + 2\alpha W)\right]\right\}\left(\frac{\emptyset}{\emptyset_y}\right) - \left[\psi W(d/t)\right]^3 = 0$$

Moment:

$$\frac{M}{M_p} = \left(\frac{\phi}{\phi_y}\right)\left(\frac{1}{f}\right) - \frac{btd}{Z}\left\{\left[\frac{\psi^3 W^2}{3\phi/\phi_y} \quad (d/t)\left(1 - \frac{\psi W}{\phi/\phi_y}\right)\right] + \right.$$

$$\left. + \left[\frac{(\phi/\phi_y)^2}{3W} \; (t/d)^2 \; \left(1 - \frac{3t}{2d}\right)\right] + \alpha^2 W(1-t/d) - \alpha(t/d) \; (\phi/\phi_y) \; \left(1 - \frac{4t}{3d}\right)\right\}$$

Limits: $\alpha_{(3)} \leqslant \alpha \leqslant \alpha_{(5)}$ or $\alpha_{(4)} \leqslant \alpha \leqslant \alpha_{(5)}$

$0 \leqslant \psi \leqslant \psi_{(5)}$ or $\psi_{(4)} \leqslant \psi \leqslant \psi_{(5)}$

where $\alpha_{(5)}$ and $\psi_{(5)}$ are defined by:

$$\psi_{(5)} = \frac{1/W + \alpha_{(5)} - 1/2}{(d/t - 1)} \quad ;$$

$$\alpha^2_{(5)} - \left[\frac{\left(\frac{1}{W} - \frac{1}{2}\right)}{(d/t-2)} + \left(1 + \frac{wd}{2bt} - \frac{w}{b}\right)\right] \alpha_{(5)} +$$

$$\frac{\left(1 + \frac{wd}{2bt} - \frac{w}{b}\right)\left[\frac{d}{t}\left(\frac{1}{W} - \frac{1}{2}\right) - \frac{T}{W}(d/t - 1)\right]}{(d/t-2)} = 0$$

Also:

$$\psi = 1/W \quad (\phi/\phi_y - 1) + (1/2 - \alpha)$$

6) Compression flange, (Fig. 8), tension flange, (Fig. 10), and web (Fig. 11), partially yielded.

Curvature:

$$\left[d/t - \alpha + \psi + \frac{wd}{2bt} - \frac{w}{b} - \left(\frac{dw}{2bt}\right)\nu\right](\phi/\phi_y) -$$

$$-\left\{W\,(d/t)\left[\left(1 + \frac{wd}{2bt} - \frac{w}{b}\right)\left(\frac{T}{W} + \alpha\right) + \left(\frac{w}{b} - \frac{wd}{2bt}\right)\left(\frac{1}{W} - \frac{1}{2}\right) + \right.\right.$$

$$\left.\left. + \alpha - \alpha^2 + \psi^2 - \left(\frac{wd}{2bt}\right)\left(\alpha + \frac{1}{W} - \frac{1}{2}\right)\nu\right]\right\} = 0$$

where $\psi = 1/W\,(\phi/\phi_y - 1) + (1/2 - \alpha)$

and $\nu = \dfrac{\psi W}{\phi/\phi_y} - t/d$

Moment:

$$\frac{M}{M_p} = \frac{btd}{Z}\left\{(1-t/d)\left[\frac{\phi}{\phi_y} - W(\alpha^2 + {}^2)\right] - t/d\left(\frac{\phi}{\phi_y}\right)\left[(1-\alpha-\psi)\left(1-\frac{4t}{3d}\right) + \right.\right.$$

$$\left.\left. + \frac{2}{3W}\left(\frac{\phi}{\phi_y}\right)(t/d)\left(1-\frac{3t}{2d}\right)\right]\right\} + \left(\frac{wd^2}{6Z}\right)\left\{\left[1 - W\left(\frac{1}{2} - \alpha\right) - t/d\left(\frac{\phi}{\phi_y}\right)\right]\left[\left(1 - \frac{2t}{d}\right)^2 + \right.\right.$$

$$\left.\left. + \nu(1 - 2t/d - 2\nu)^2\right]\right\}$$

Limits: $\alpha_{(5)} \leqslant \alpha \leqslant 0.5$

7) All of the top flange has just yielded.

(Note that this is not a range, but only a point condition. For bottom flange and web see Fig. 10 and 11.)

Curvature:

$$\left(\frac{\phi}{\phi_y}\right)^2 + \left[(d/t)\,(3W/2)\,(1 - 2\psi)\right]\left(\frac{\phi}{\phi_y}\right) + (3W/2)\,(d/t)^2\left[2\psi W(\psi - 1) - \right.$$

$$\left. -2\,(1-T) + \frac{3W}{2} + \frac{wd}{bt}\left(1 - \frac{2t}{d}\right)\left(1 - \nu\right)\frac{wd\nu}{bt}\right] = 0$$

where $\psi = \frac{1}{W}\left[(1-t/d)\ \frac{\emptyset}{\emptyset_y} - 1\right]$

and $\nu = (1 - \frac{2t}{d}) - \frac{1}{(\emptyset/\emptyset_y)}$

Moment:

$$\frac{M}{M_p} = \frac{btd}{Z}\left\{(1-t/d)\left[1+W\ (\psi-\psi^2 - \frac{1}{4})\right] - \frac{1}{2}\ (t/d)\ (\emptyset/\emptyset_y)\ (1-2\psi)(1-\frac{4t}{3d}) - \right.$$

$$\left. - \frac{1}{3}(t/d)^2\left(\frac{\emptyset}{\emptyset_y}\right)^2\left(\frac{1}{W}\right)\left(1-\frac{3t}{2d}\right)\right\} + \frac{wd^2}{6Z}\ (1-\frac{2t}{d} - \nu)\ (1-\frac{2t}{d} + 2\nu)$$

8) All of outside face of bottom flange yielded.

(Note, this is not a range, but a point condition, i.e. $\psi = 0.5$. For web, see Fig. 11).

Curvature:

$$\left(\frac{\emptyset}{\emptyset_y}\right)^3 + 3W\ (d/t)^2\left[(2-U)\left(\frac{wd}{2bt}\right) - \frac{1}{2}\ (U-T) - w/b\ (1-U)\right]\frac{\emptyset}{\emptyset_y} -$$

$$-(1+W)\ (3W)\ (d/t)^2\left(\frac{wd}{2bt}\right) = 0$$

Moment:

$$\frac{M}{M_p} = \frac{btd}{Z}\left\{(1-t/d) - \left(\frac{1}{3W}\right)(t/d)^2\left(\frac{\emptyset}{\emptyset_y}\right)^2\ (1-\frac{3t}{2d})\right\} +$$

$$+ \frac{wd^2}{6Z}\left\{\left(\frac{3}{\emptyset/\emptyset_y}\right)(1+W) - \frac{1}{(\emptyset/\emptyset_y)^2}\left(2 + 3W + \frac{3W^2}{2}\right) - 6(t/d)(1-t/d)\right\}$$

APPENDIX B

SECTION	D_T	SECTION	D_T	SECTION	D_T
26WF300	578	21WF 73	334	14WF 43	447
230	354	62	246	38	386
194	312	18WF114	867	30	242
150	190	96	646	12WF190	4329
33WF240	496	85	695	106	1785
200	356	64	426	65	786
152	263	60	408	58	842
130	188	50	281	53	709
30WF210	539	16WF 96	899	50	830
172	376	88	769	40	578
132	291	78	833	36	568
108	190	58	497	27	343
27WF177	555	50	418	10WF112	3600
145	394	36	222	72	1809
114	256	14WF426	7757	49	966
27WF 94	219	246	3712	45	1130
24WF160	621	142	1580	33	639
130	421	320	5147	29	696
120	423	136	1570	21	329
100	309	111	1124	8WF 67	3221
94	342	87	742	31	925
76	305	84	901	28	1010
21WF142	793	78	766	24	789
112	521	74	895	20	590
96	544	61	640	17	500
82	412	53	630		

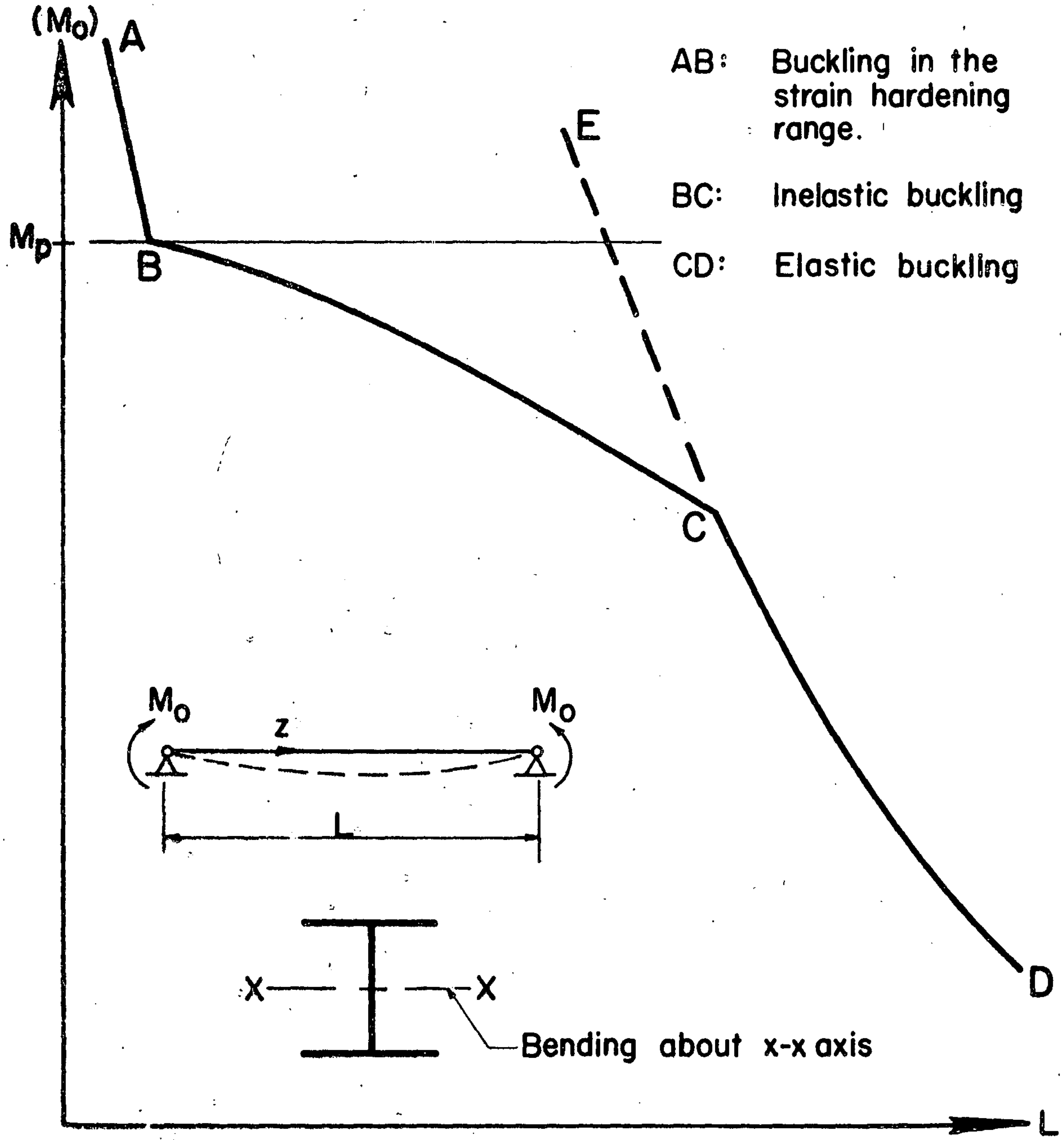

Fig. 1 MOMENT-VERSUS-LENGTH CURVE FOR SIMPLY SUPPORTED BEAM

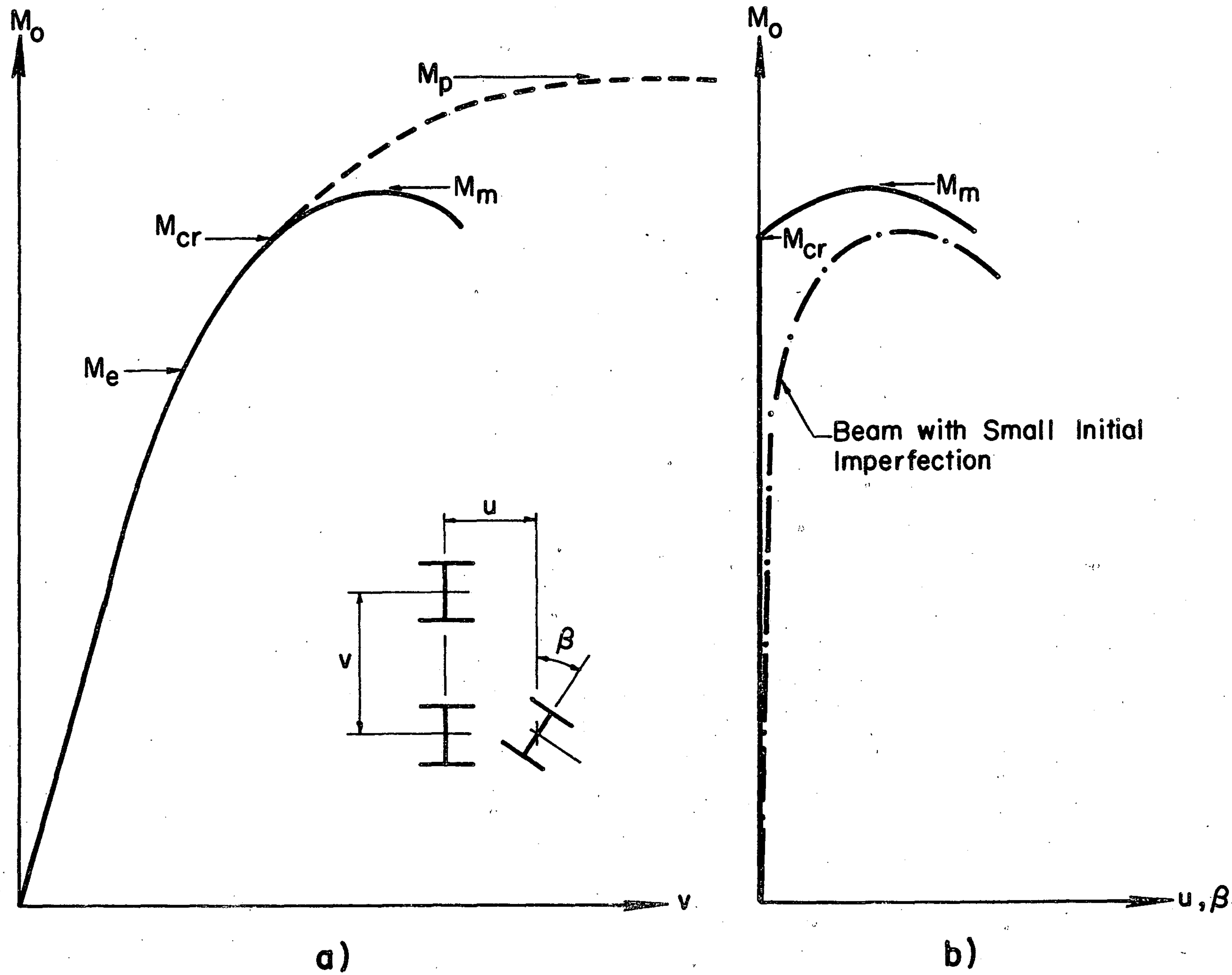

Fig. 2 ILLUSTRATION OF THE NATURE OF LATERAL BUCKLING

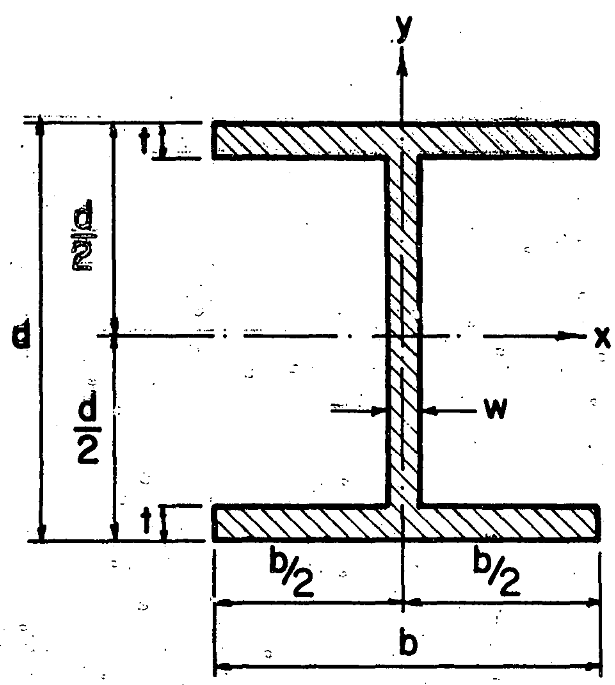

Fig. 3 THE IDEALIZED WIDE-FLANGE CROSS SECTION

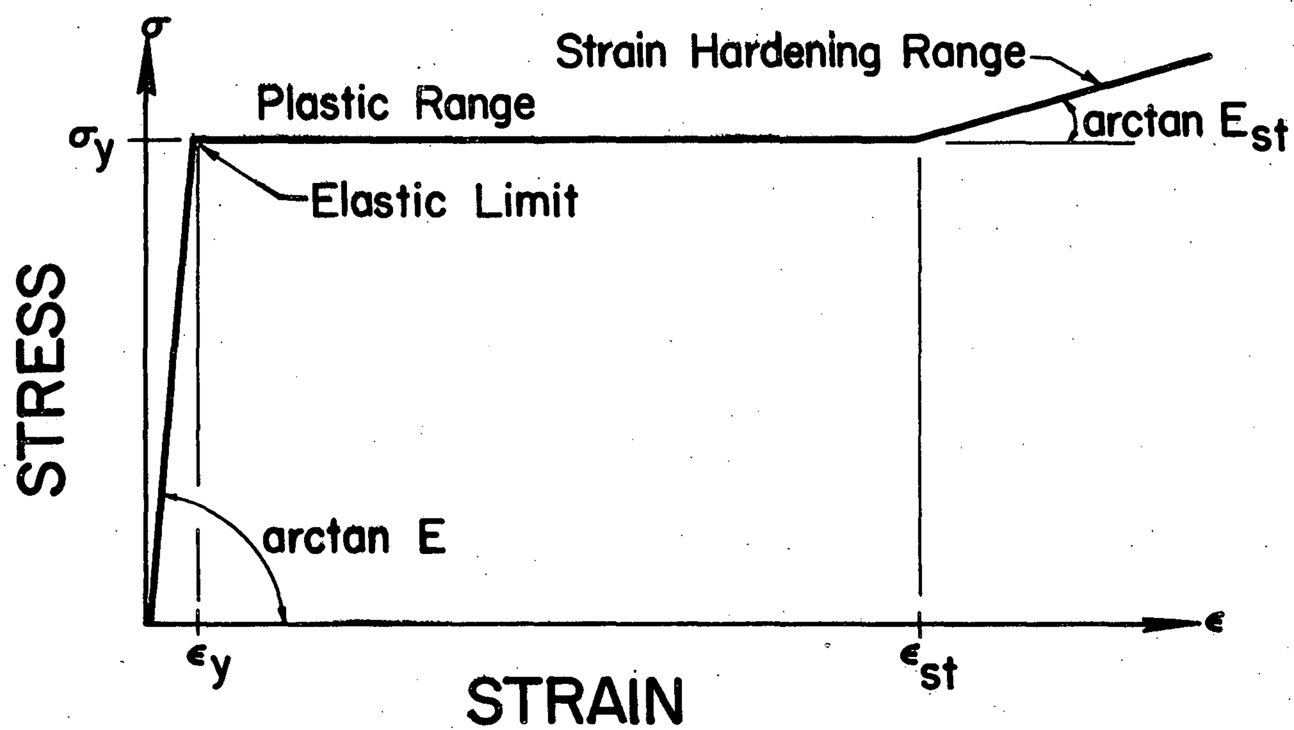

Fig. 4 IDEALIZED STRESS-STRAIN DIAGRAM IN TENSION AND COMPRESSION

$$\sigma_{rc} = 0.3\,\sigma_y$$

$$\sigma_{rt} = \left[\frac{bt}{bt+w(d-2t)}\right]\sigma_{rc}$$

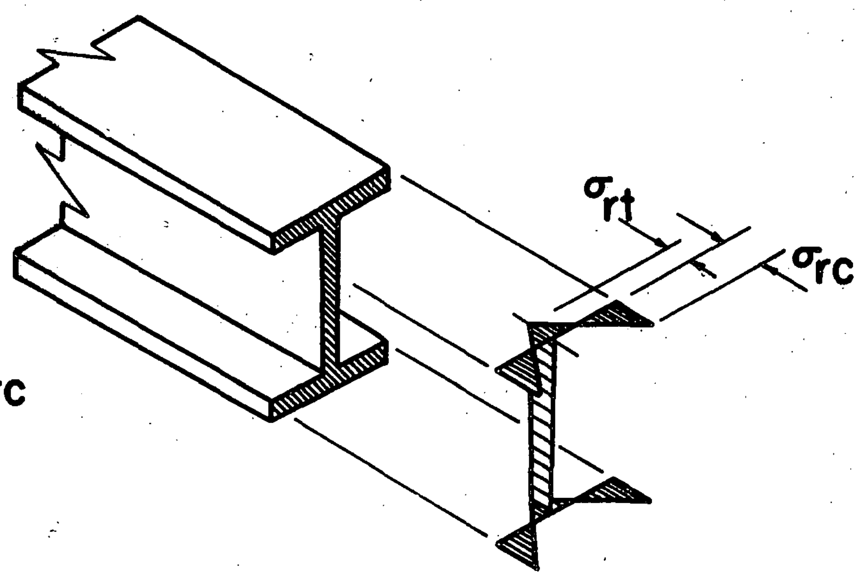

Fig. 5 ASSUMED RESIDUAL STRESS PATTERN

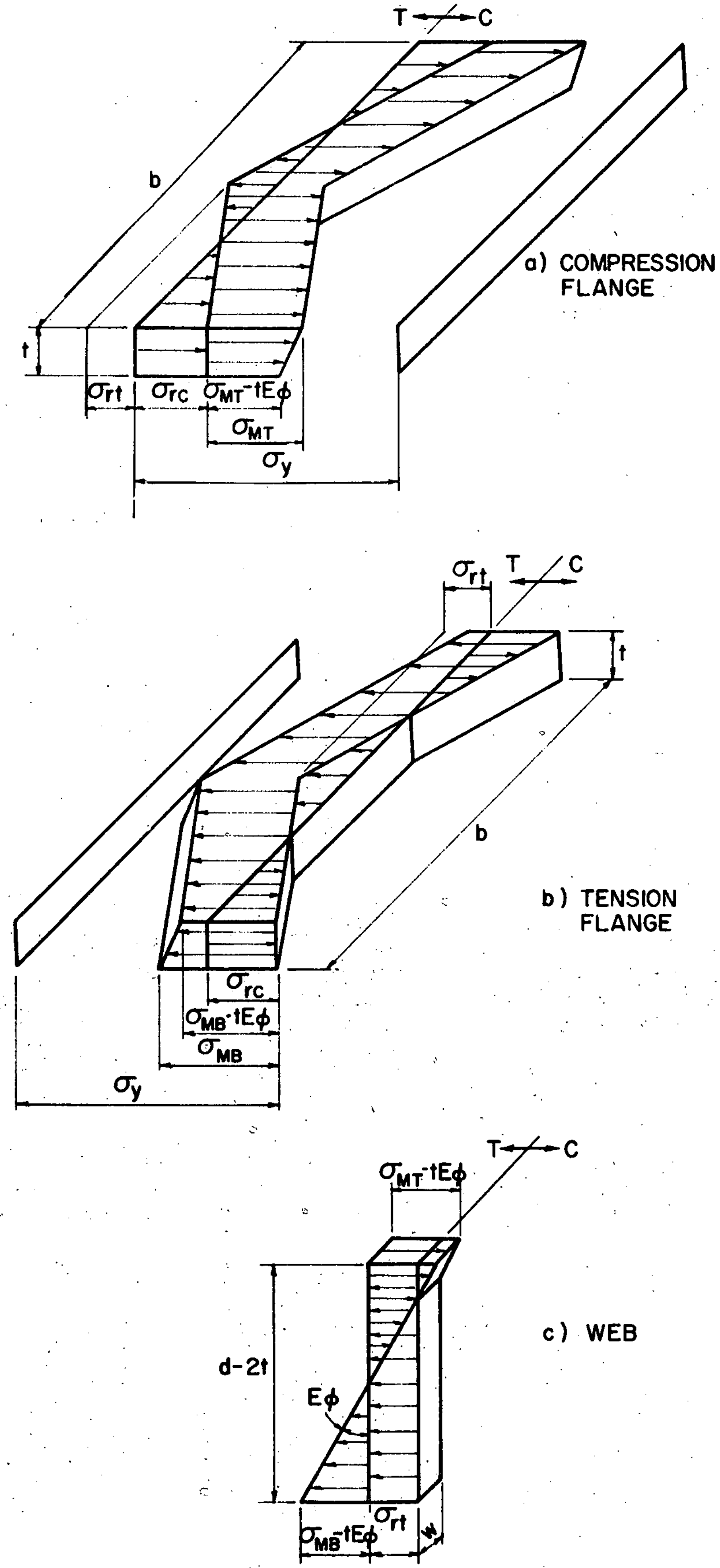

Fig. 6 STRESS DISTRIBUTION IN THE ELASTIC RANGE

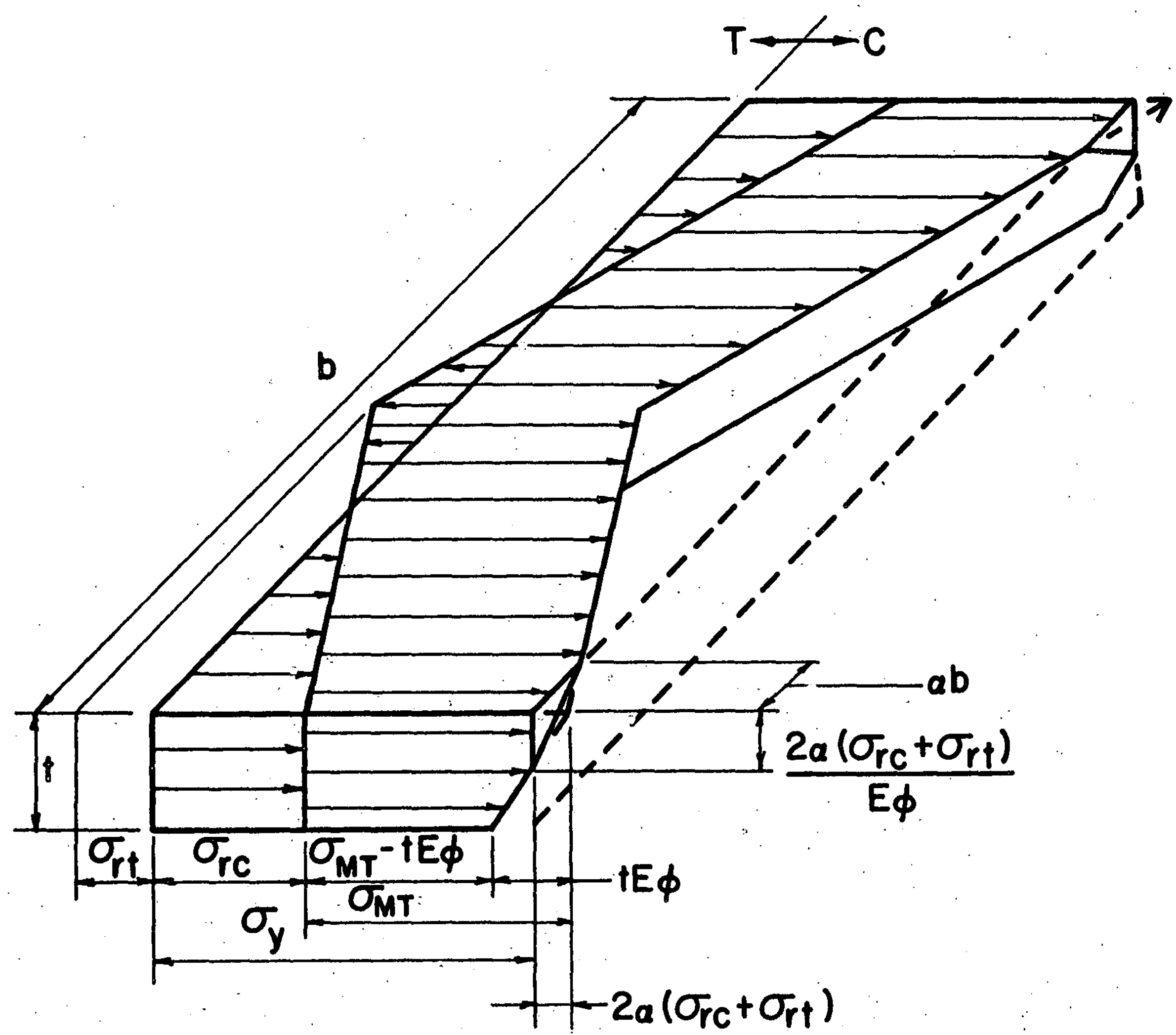

Fig. 7 COMPRESSION FLANGE PARTIALLY YIELDED $\left[tE\phi > 2\alpha(\sigma_{rc} + \sigma_{rt}) \right]$

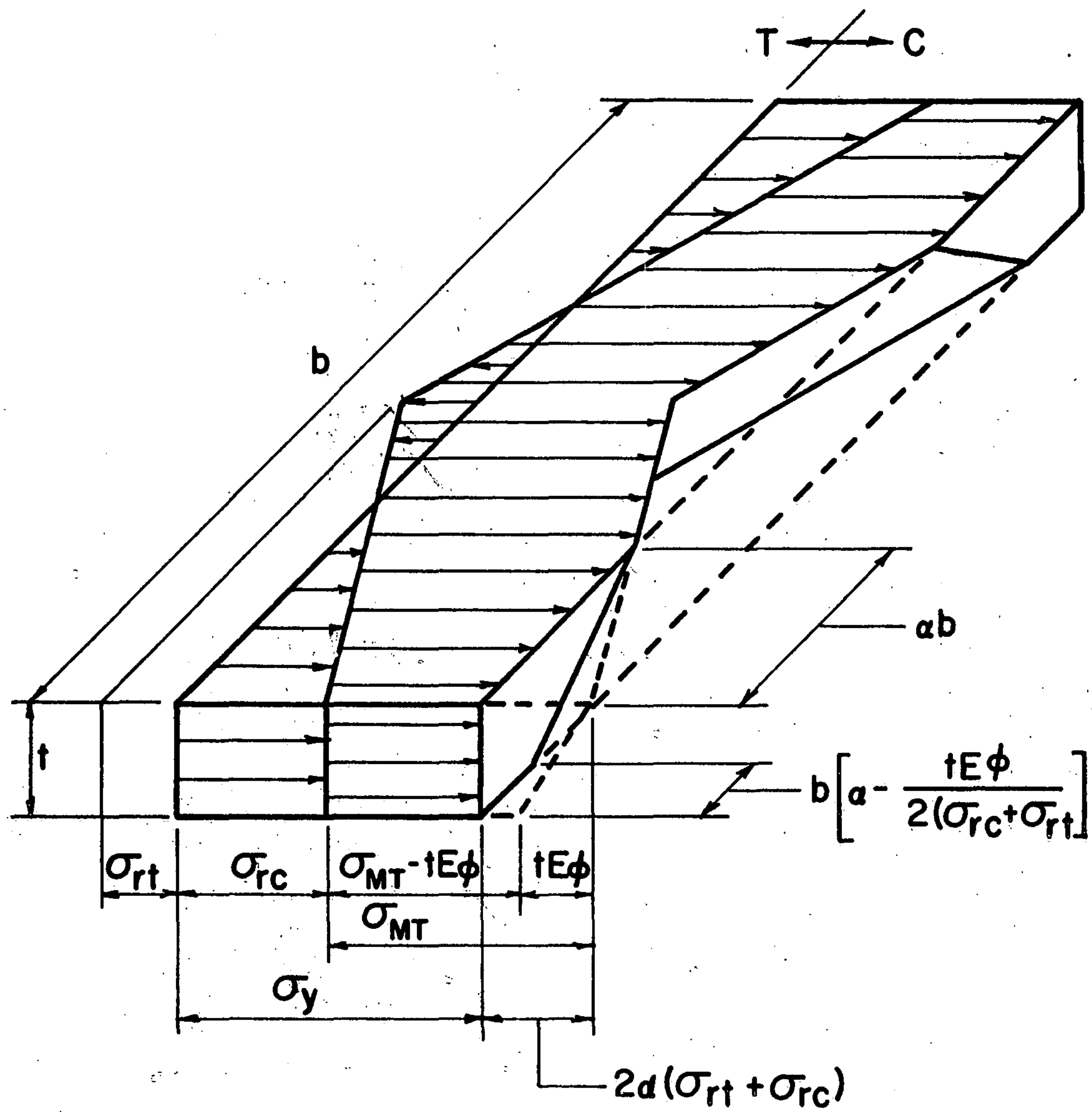

Fig. 8 COMPRESSION FLANGE PARTIALLY YIELDED $\left[tE\phi \leq 2\alpha(\sigma_{rc}+\sigma_{rt})\right]$

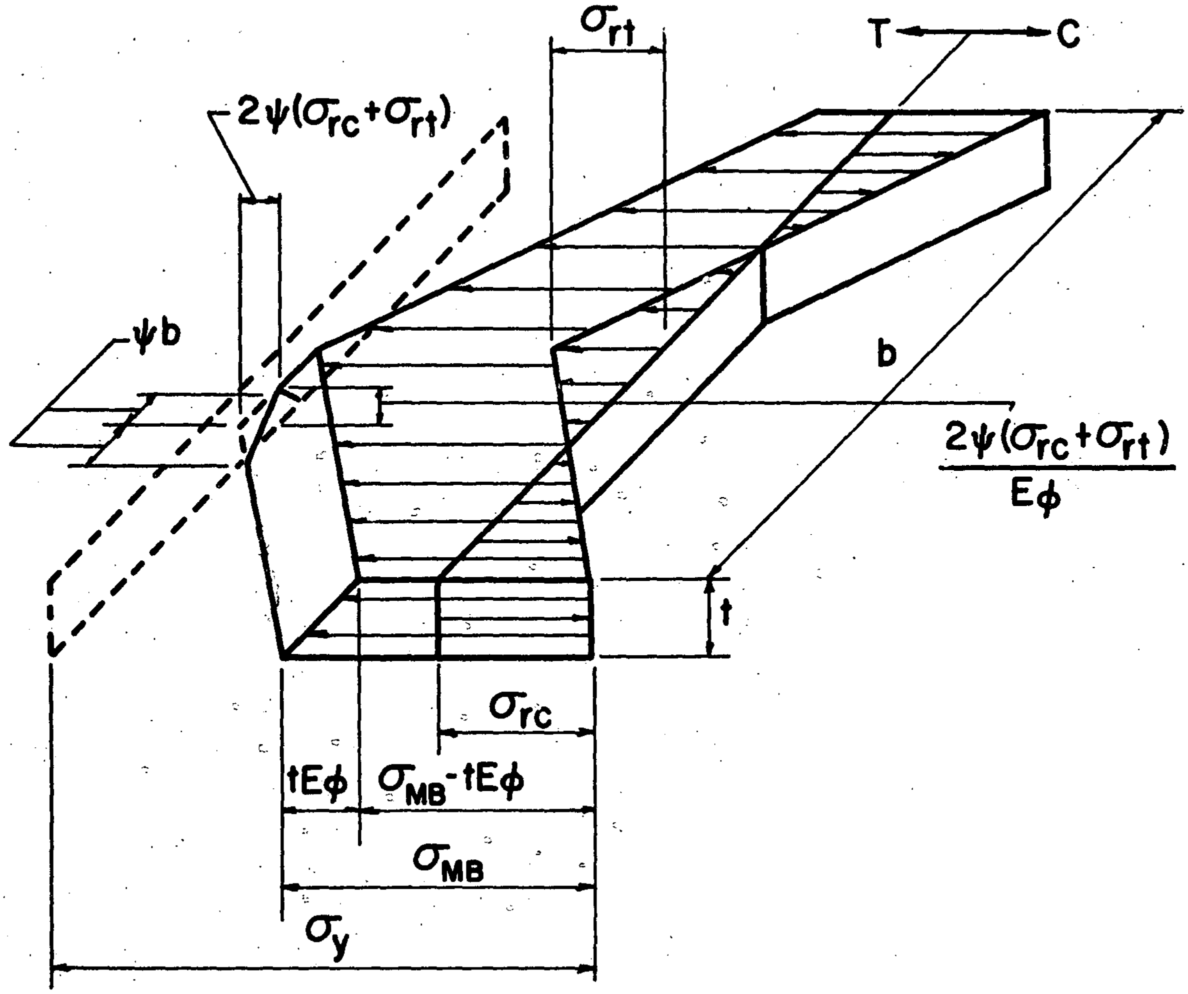

Fig. 9 TENSION FLANGE PARTIALLY YIELDED $\left[tE\phi > 2\psi(\sigma_{rc}+\sigma_{rt})\right]$

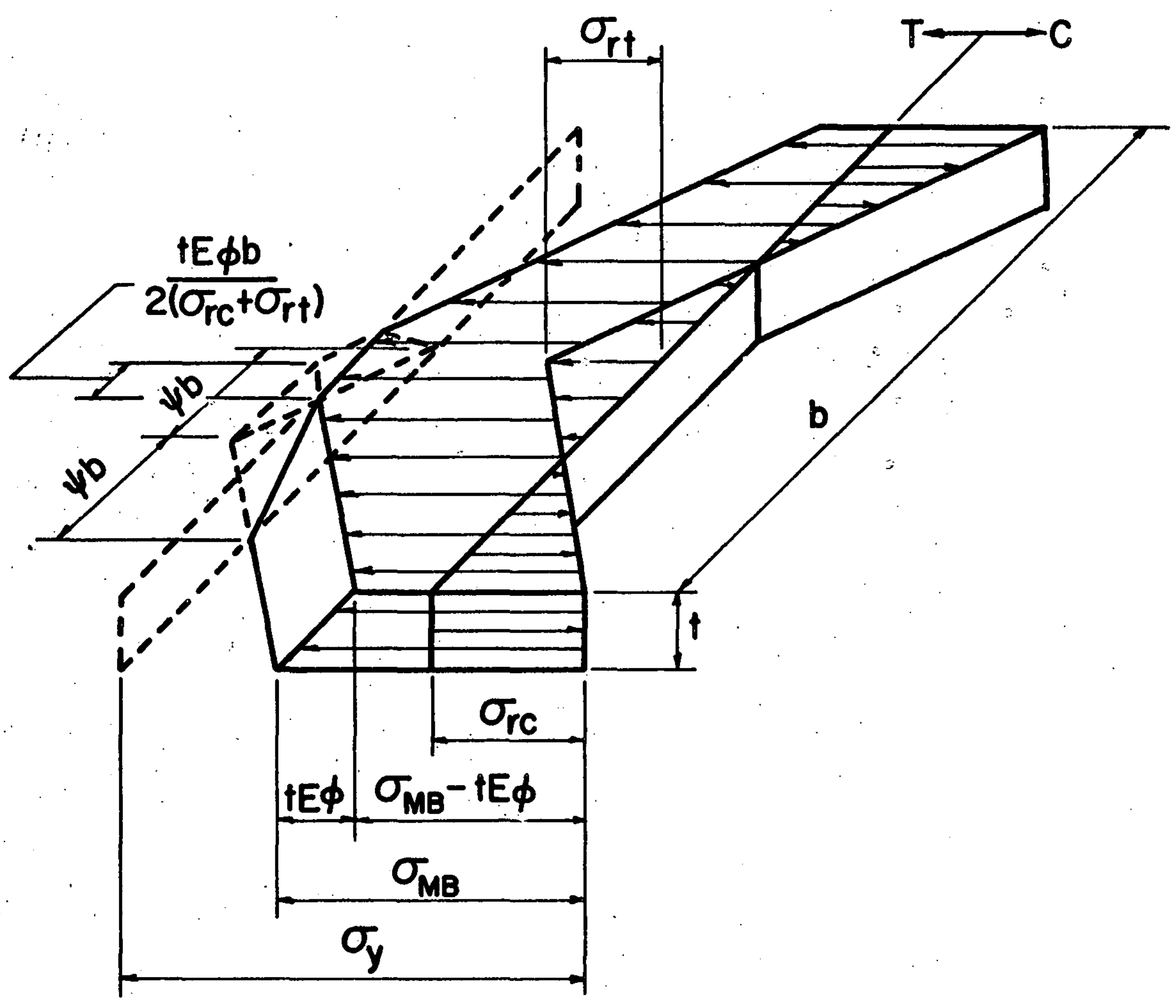

Fig. 10 TENSION FLANGE PARTIALLY YIELDED $\left[tE\phi < 2\psi(\sigma_{rc}+\sigma_{rt})\right]$

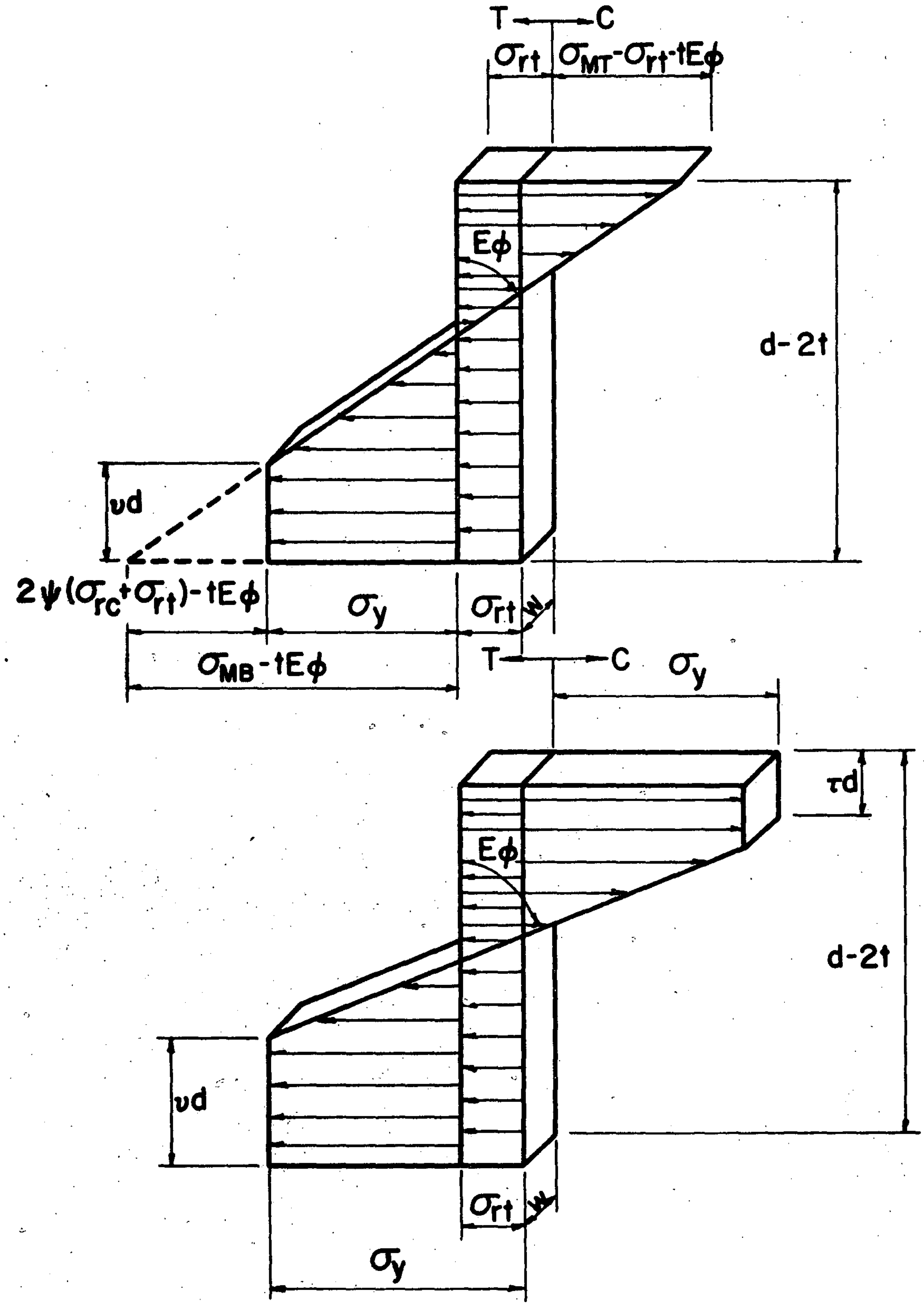

Fig. 11 WEB PARTIALLY YIELDED

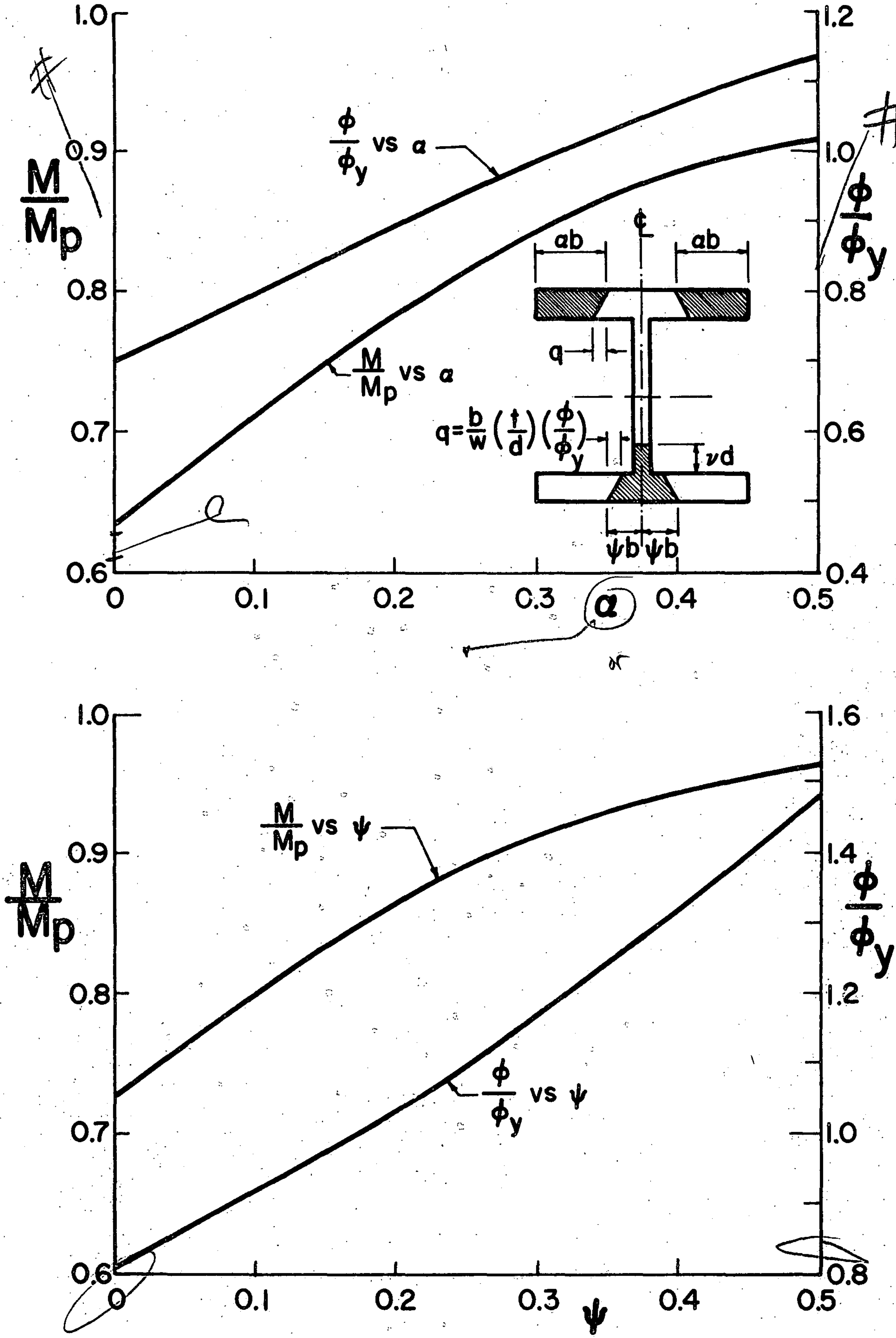

Fig. 12 MOMENT AND CURVATURE VERSUS TENSION AND COMPRESSION FLANGE YIELDING (8WF31)

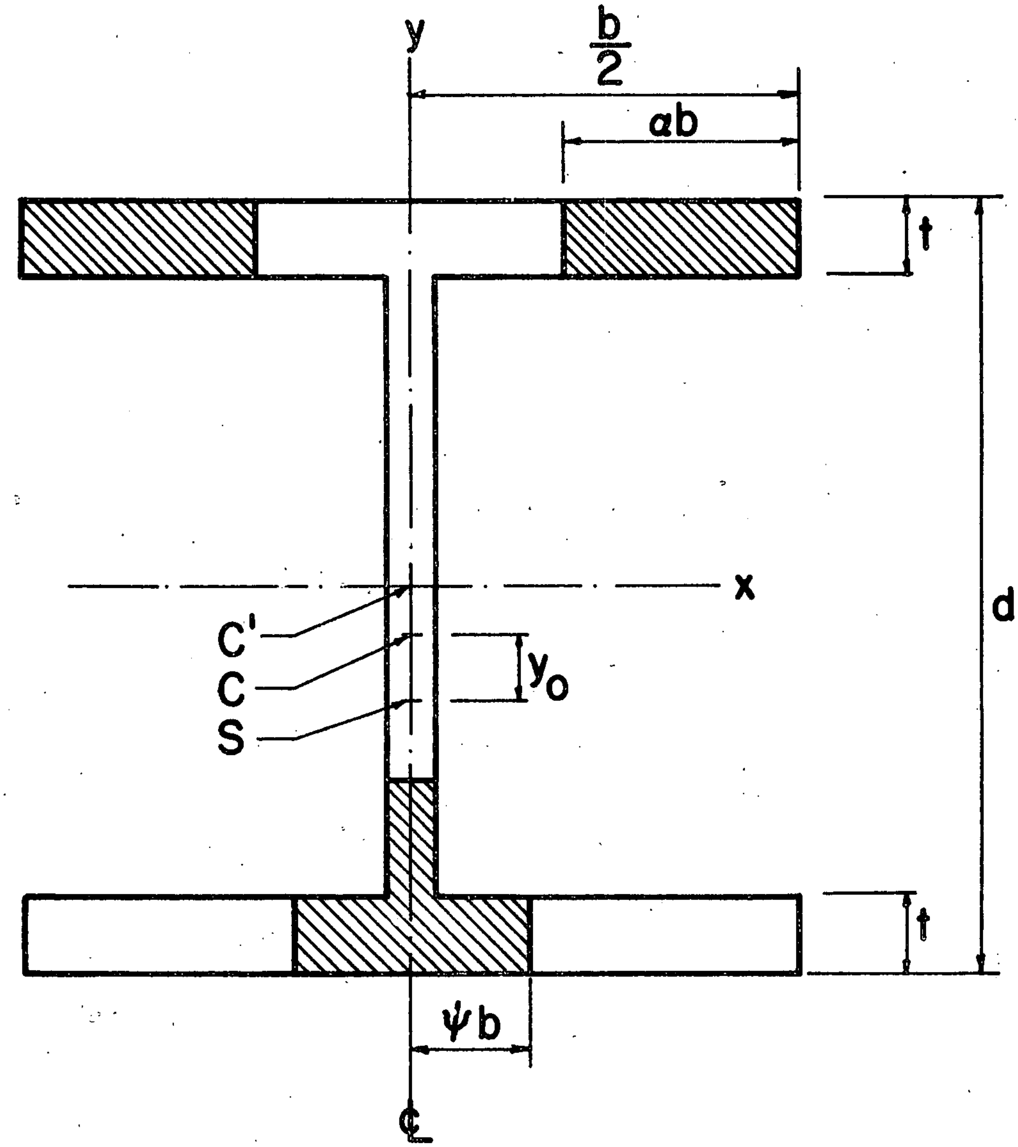

Fig. 13 THE "EFFECTIVE" CROSS SECTION

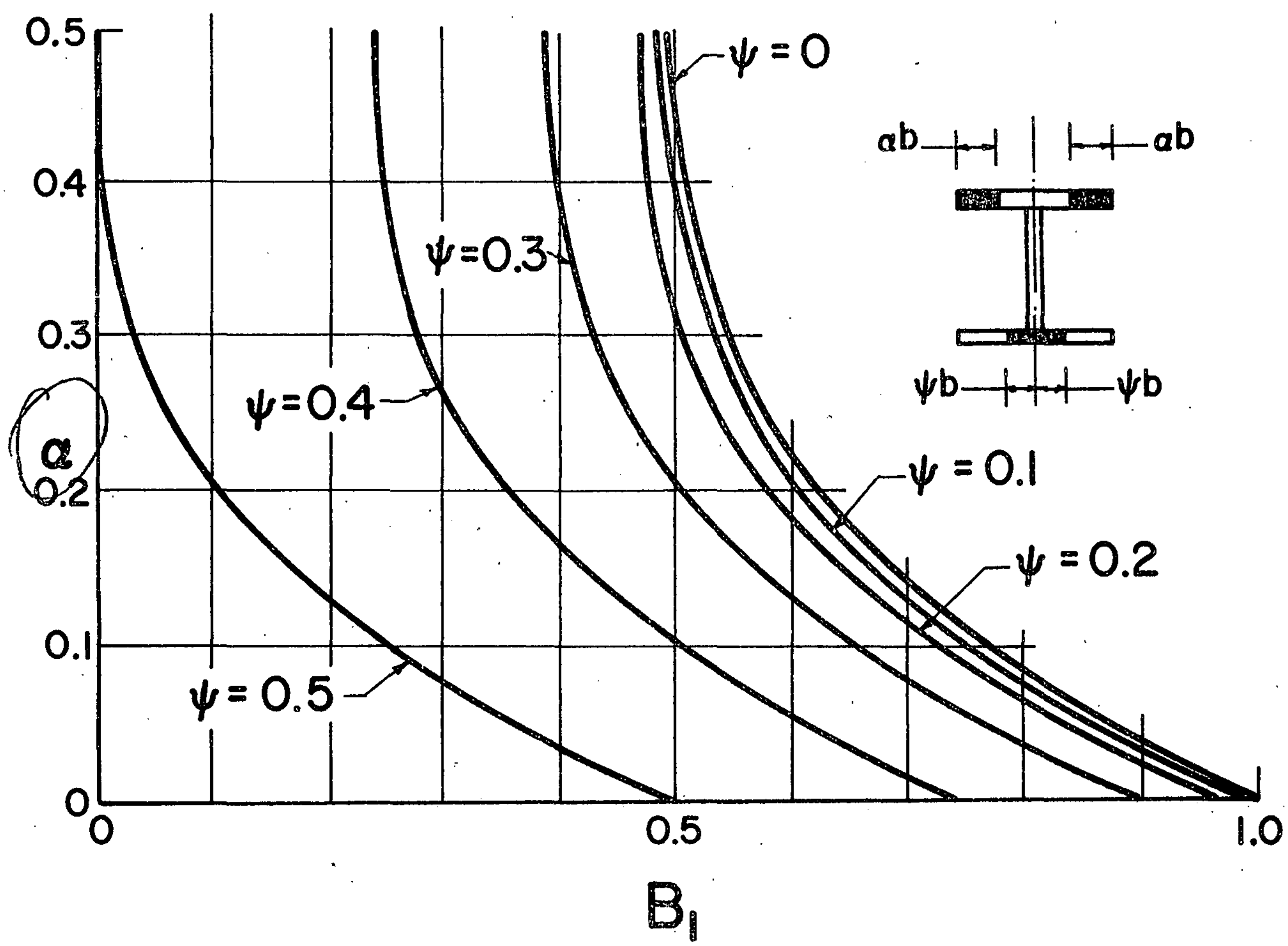

Fig. 14 BENDING STIFFNESS OF THE YIELDED CROSS SECTION

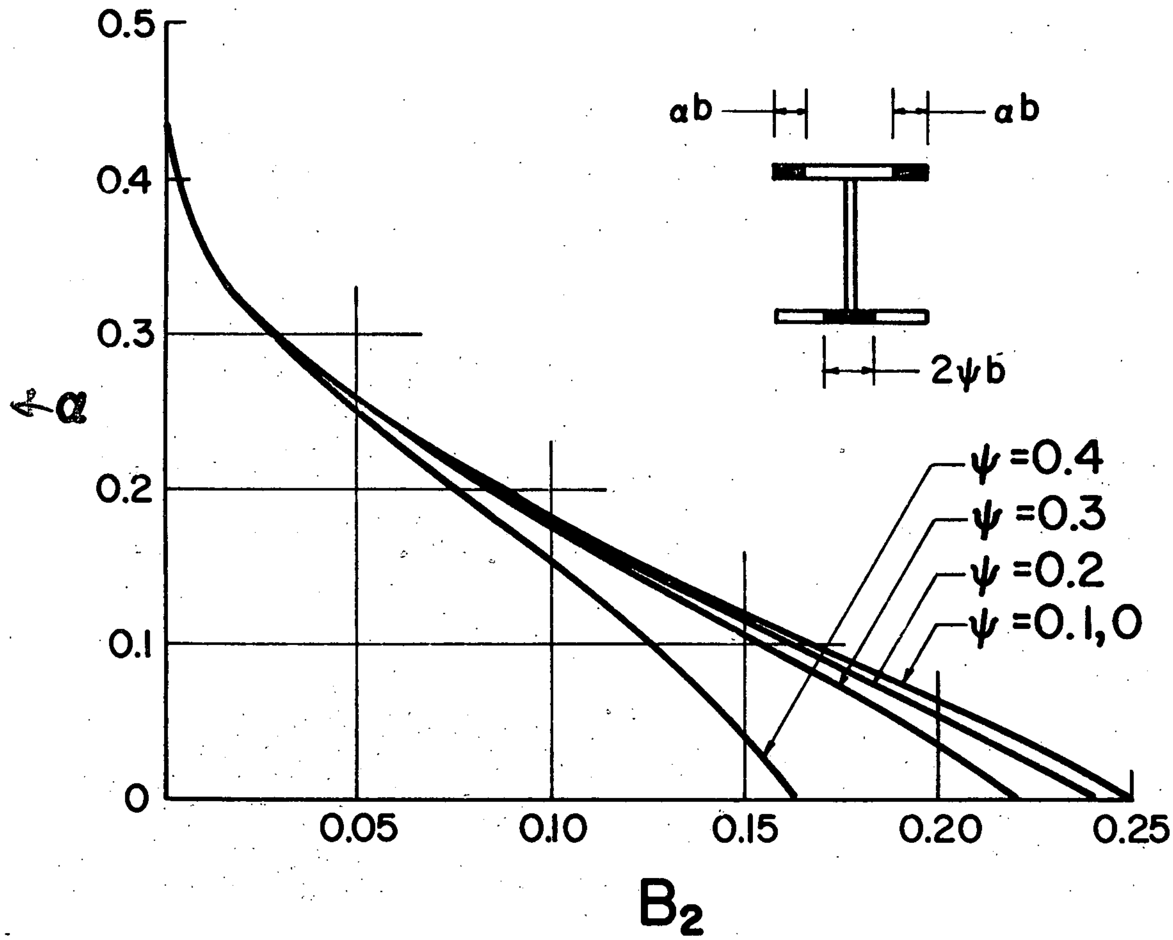

Fig. 15 WARPING STIFFNESS OF THE YIELDED CROSS SECTION

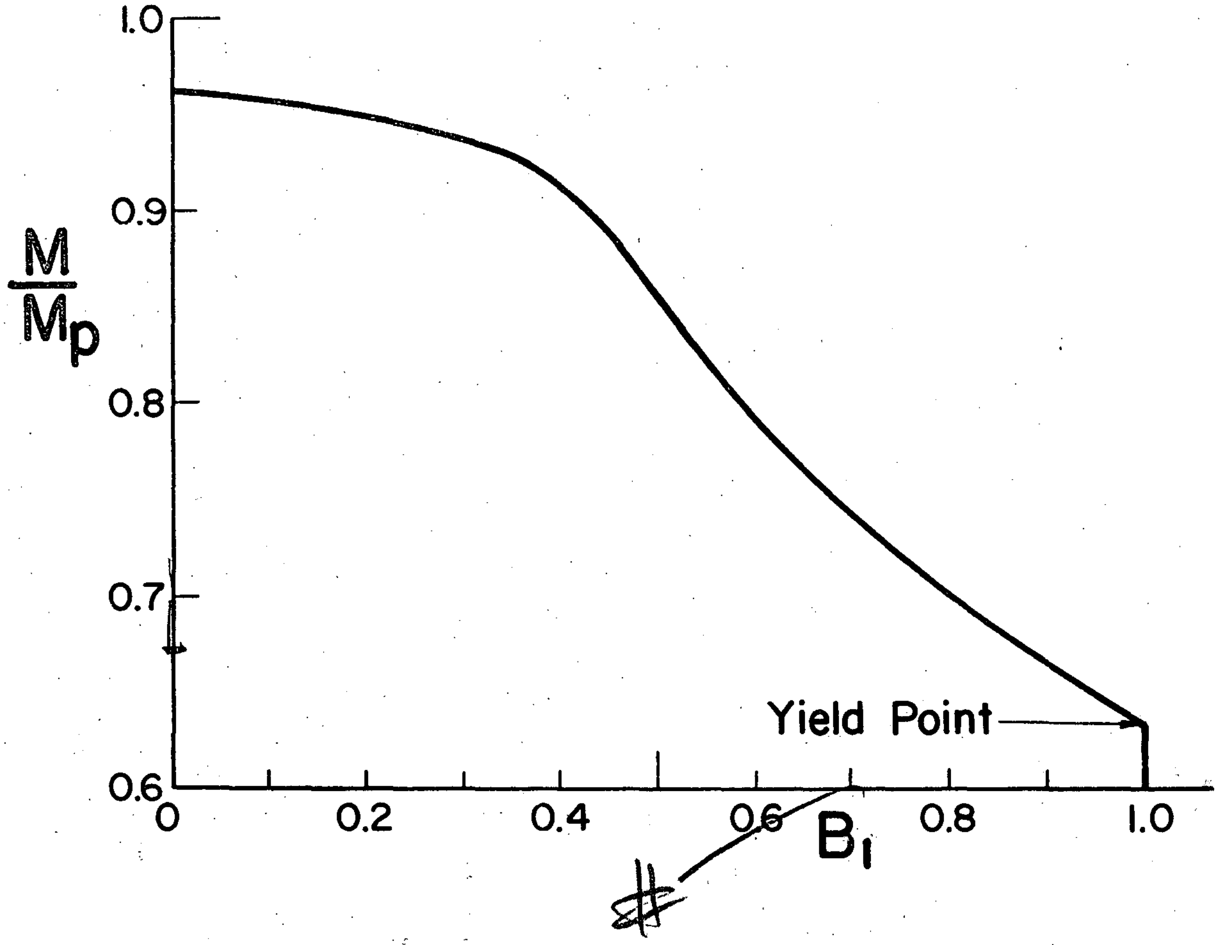

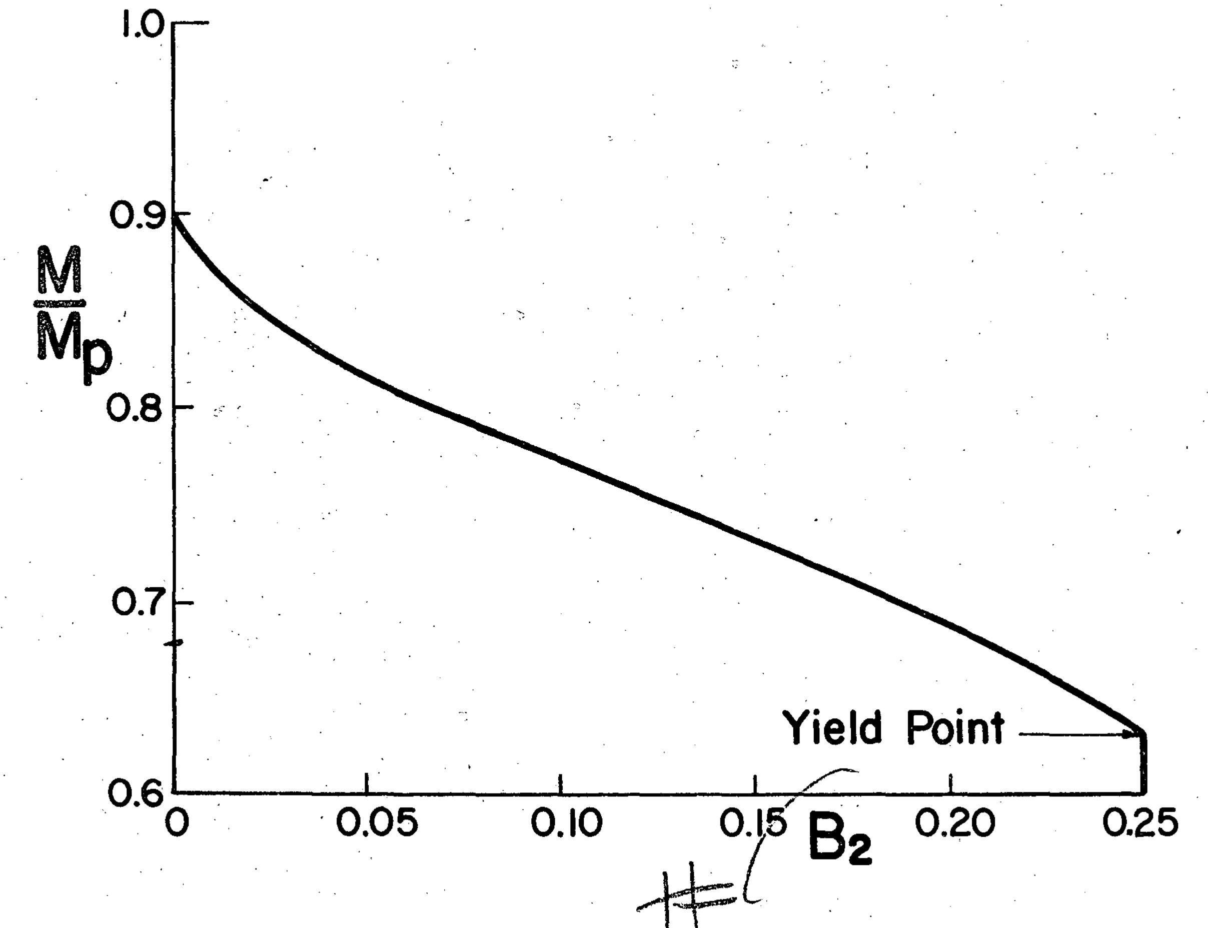

Fig.16 MOMENT - VERSUS - BENDING AND WARPING STIFFNESS

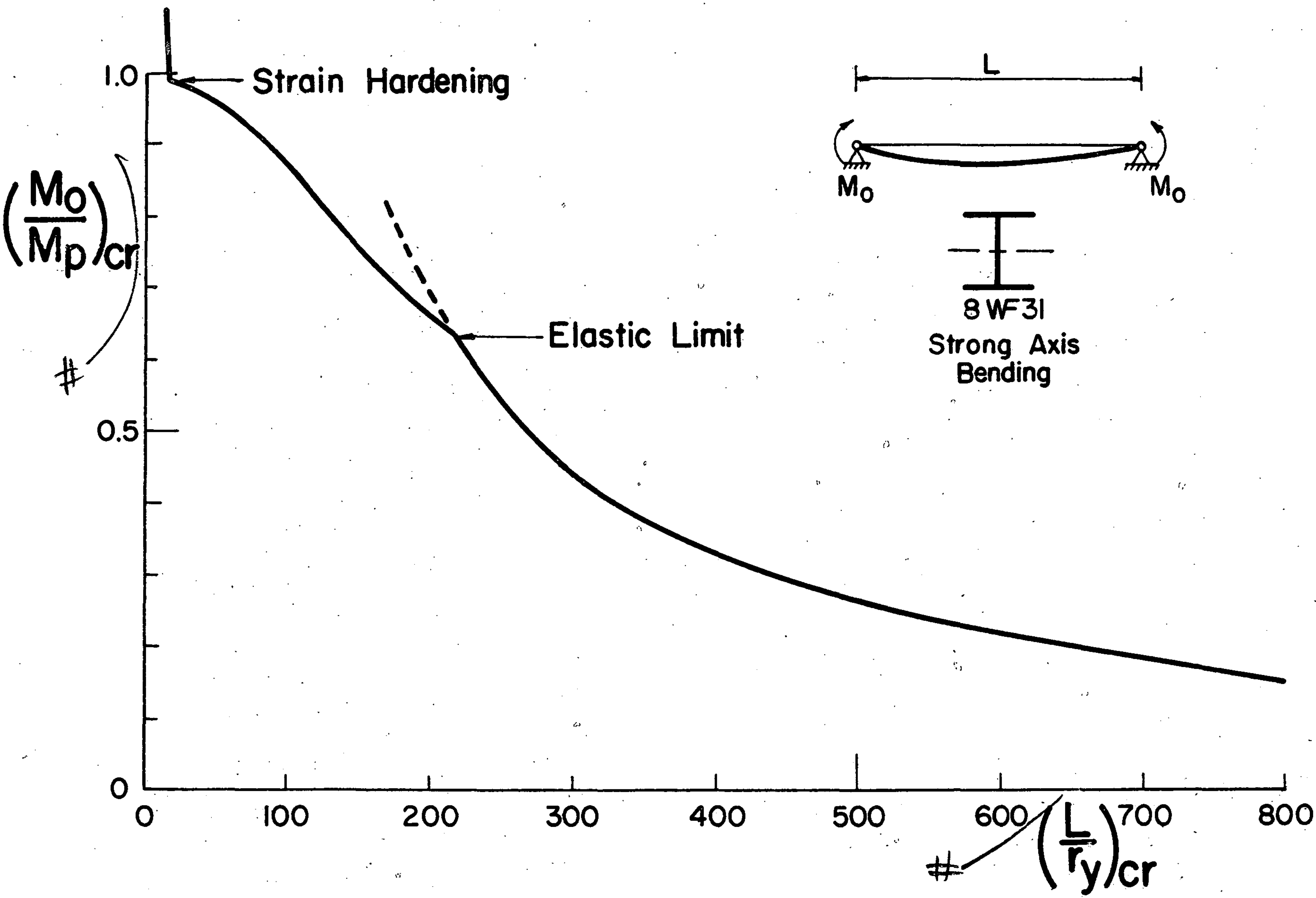

Fig. 17 BUCKLING CURVE FOR 8WF31 SECTION

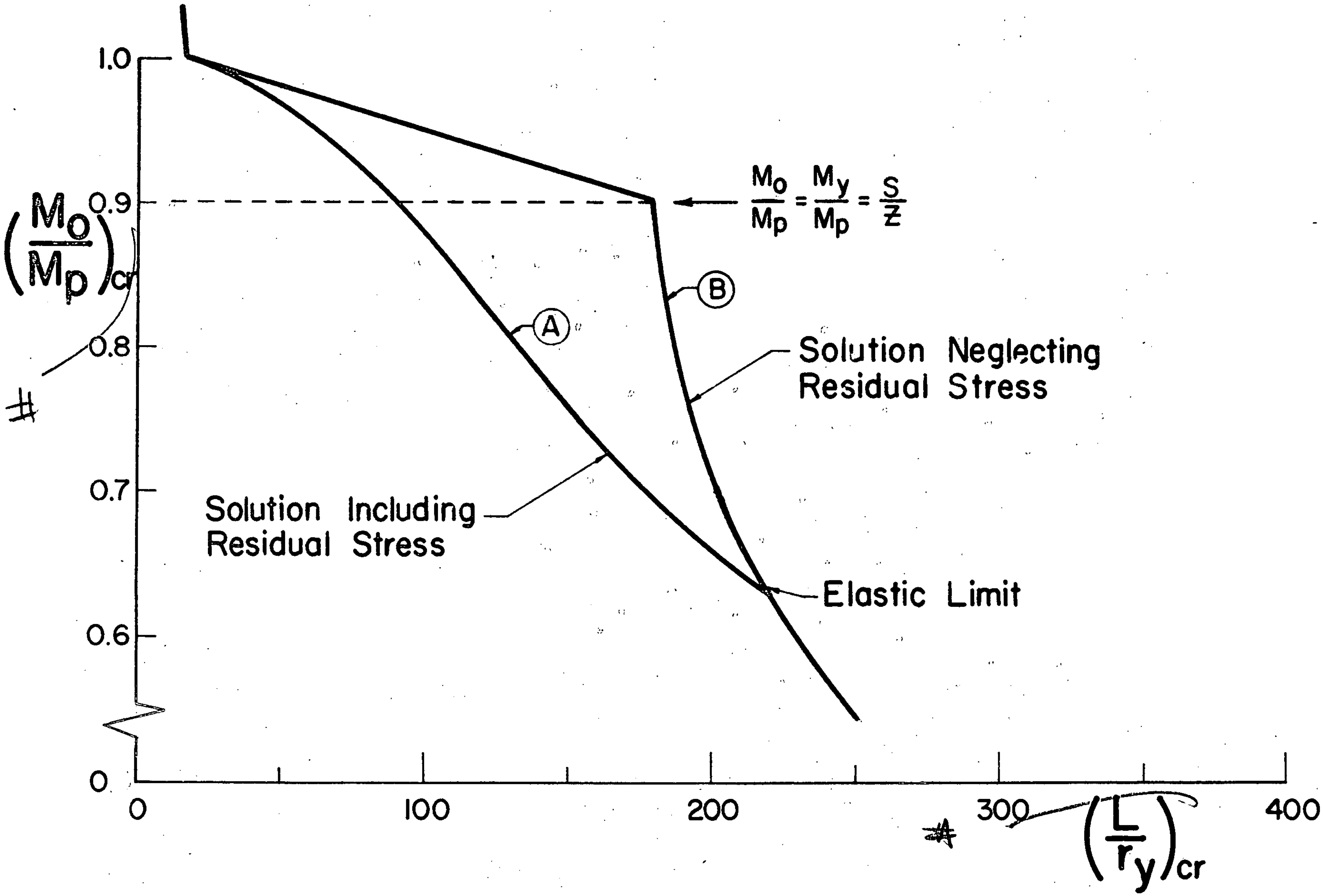

Fig. 18 INFLUENCE OF RESIDUAL STRESS ON LATERAL BUCKLING (8WF31)

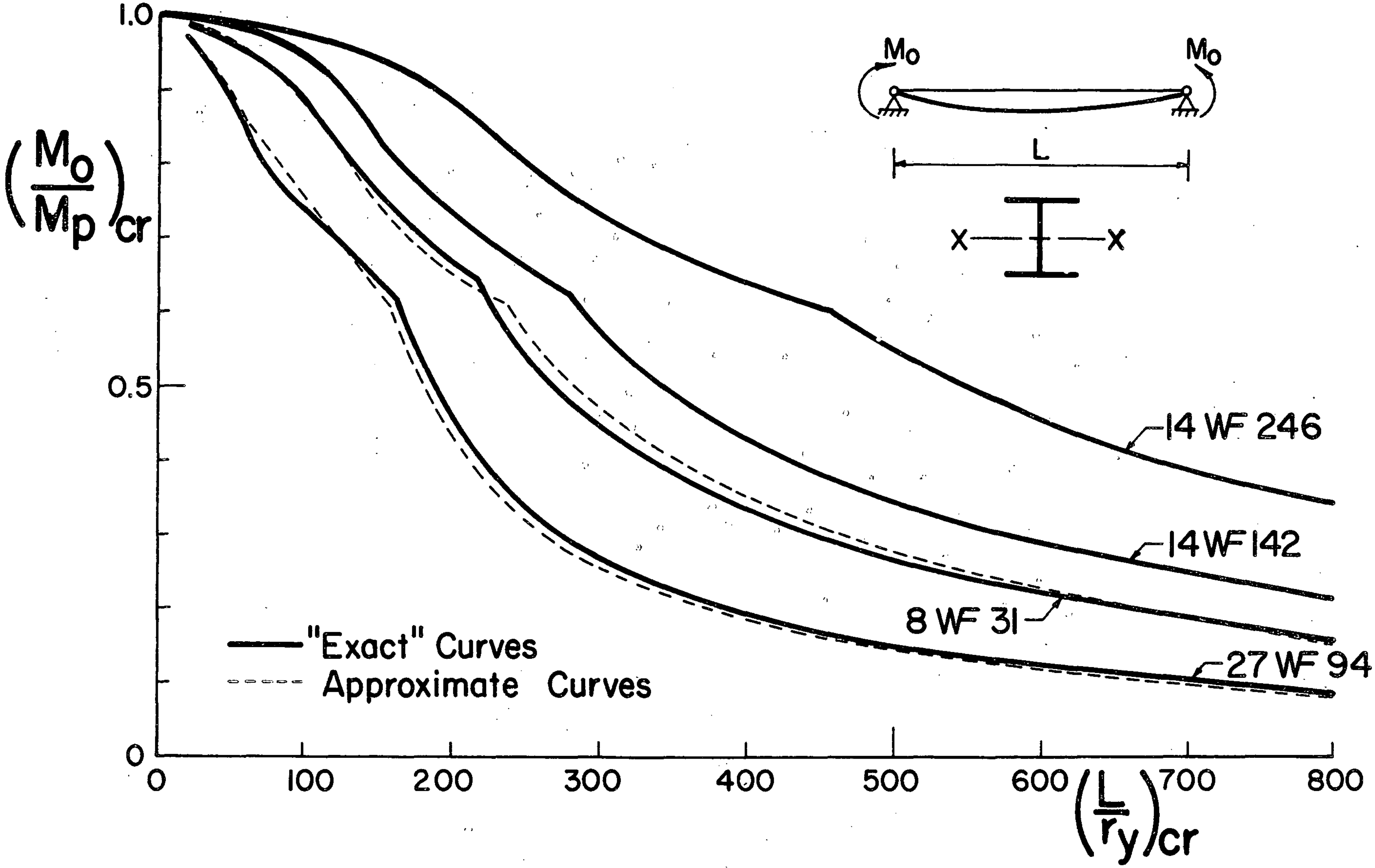

Fig. 19 LATERAL BUCKLING CURVES FOR WIDE-FLANGE SECTIONS

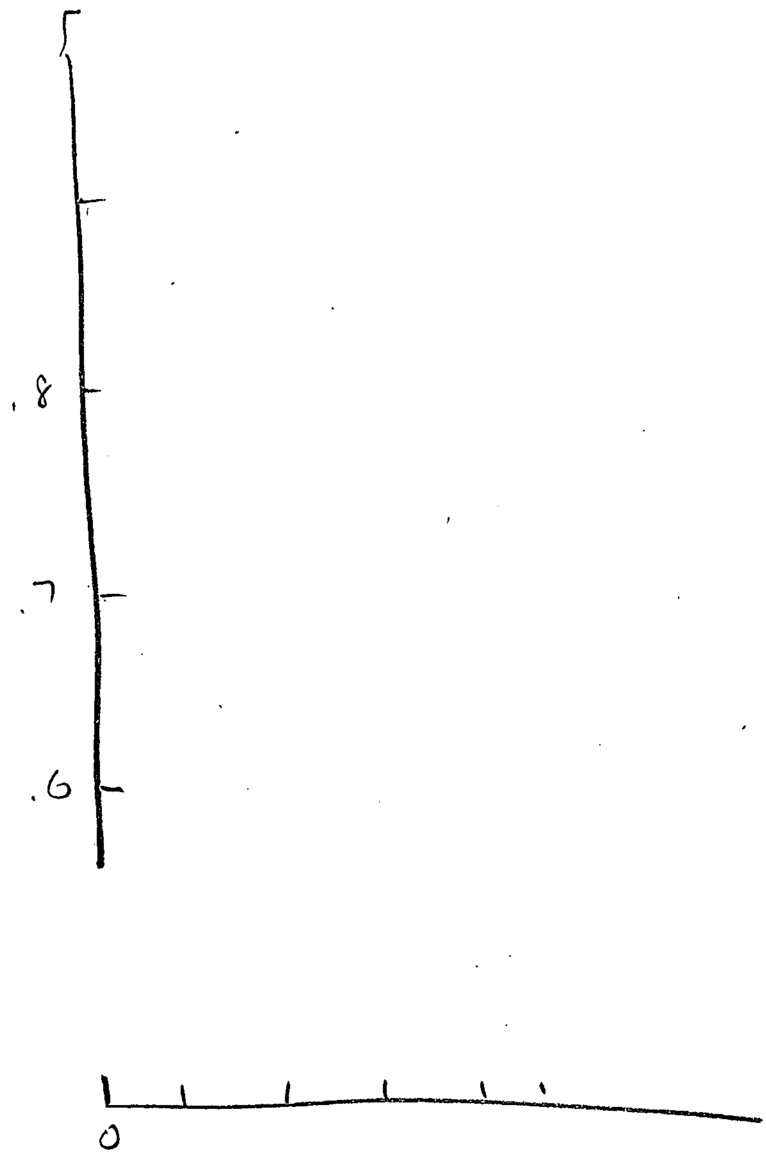
.8
.7
.6
0

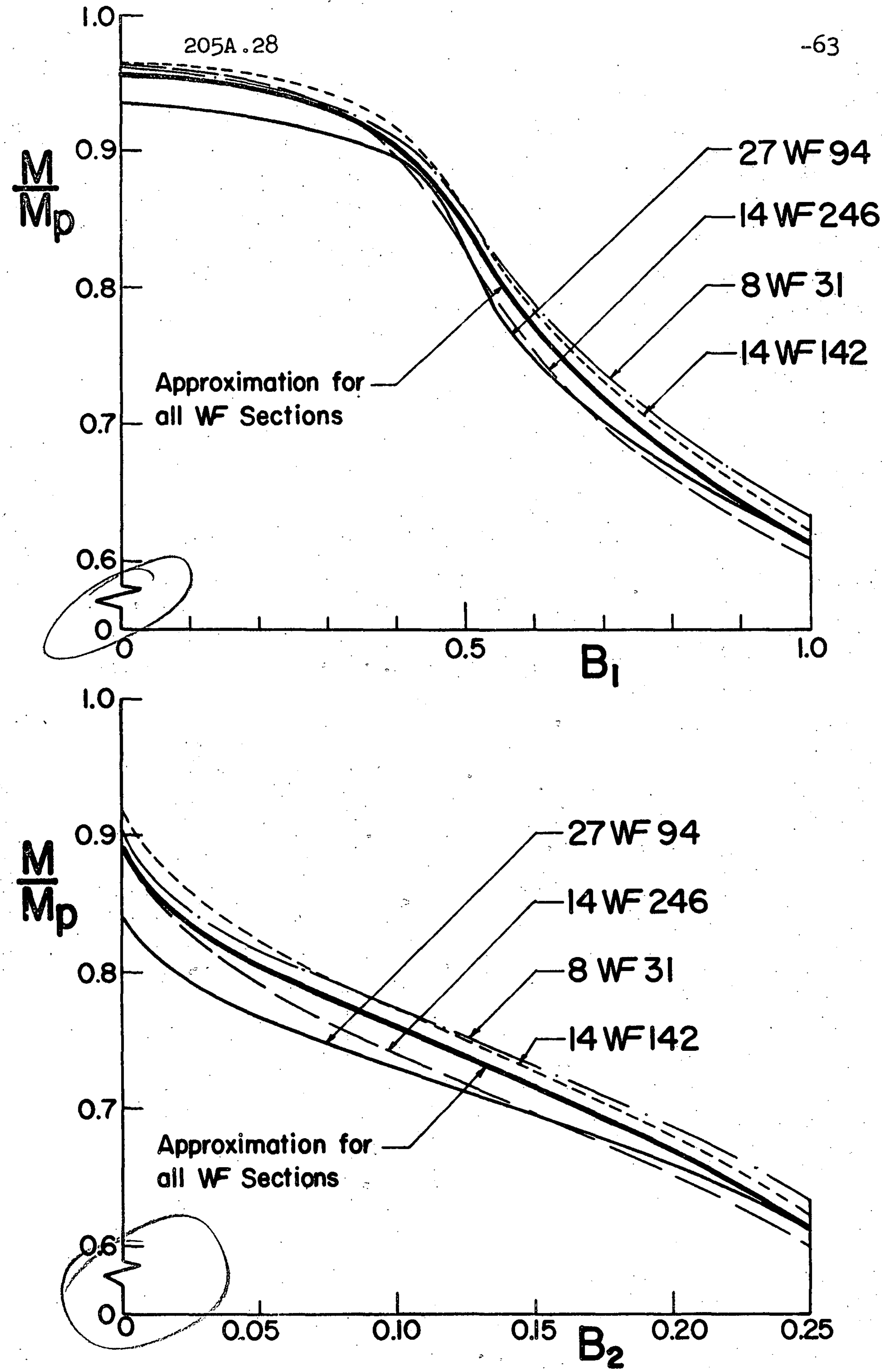

Fig. 20 AVERAGE STIFFNESS REDUCTION CURVES

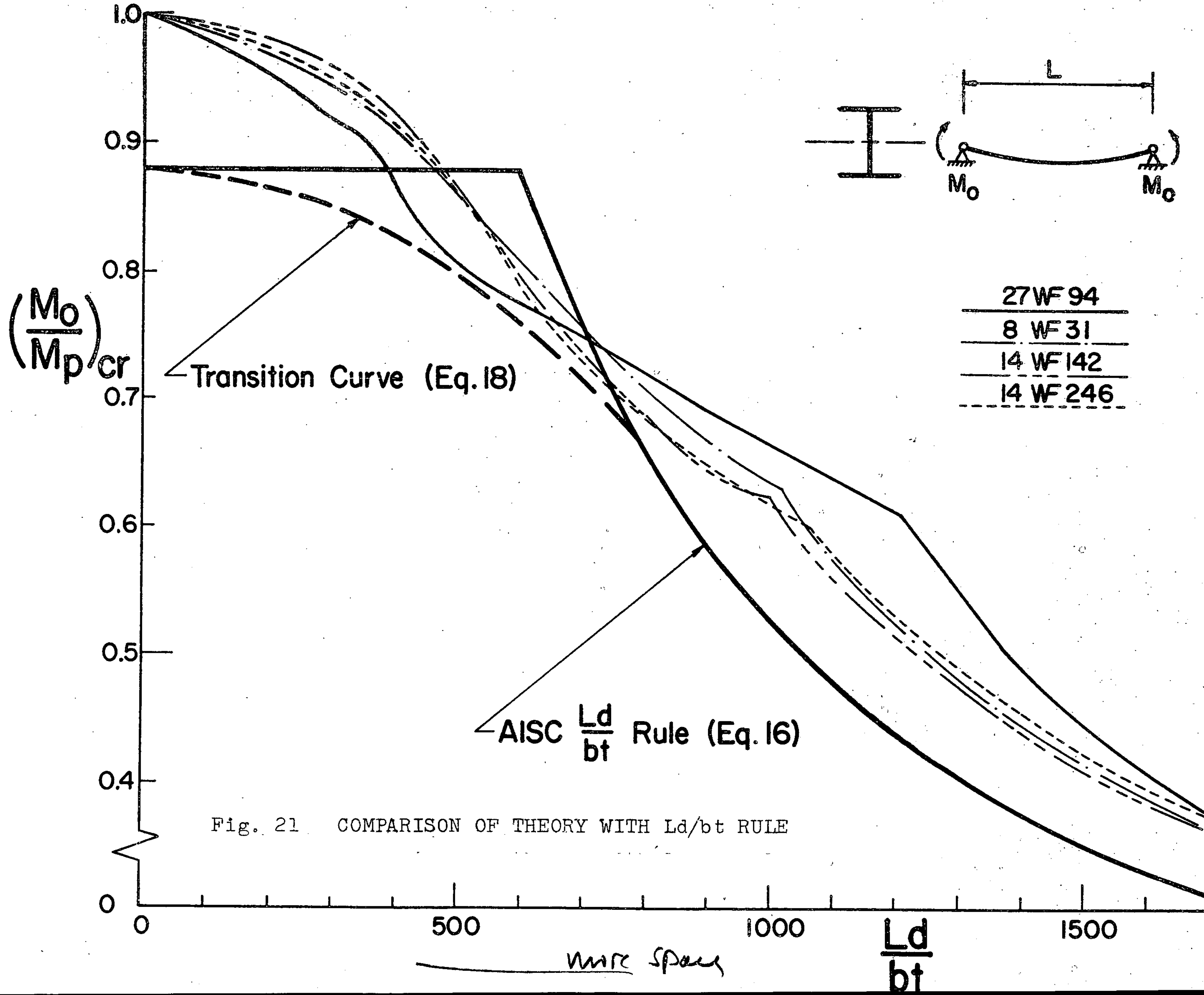

Fig. 21 COMPARISON OF THEORY WITH Ld/bt RULE

More space

205A.28

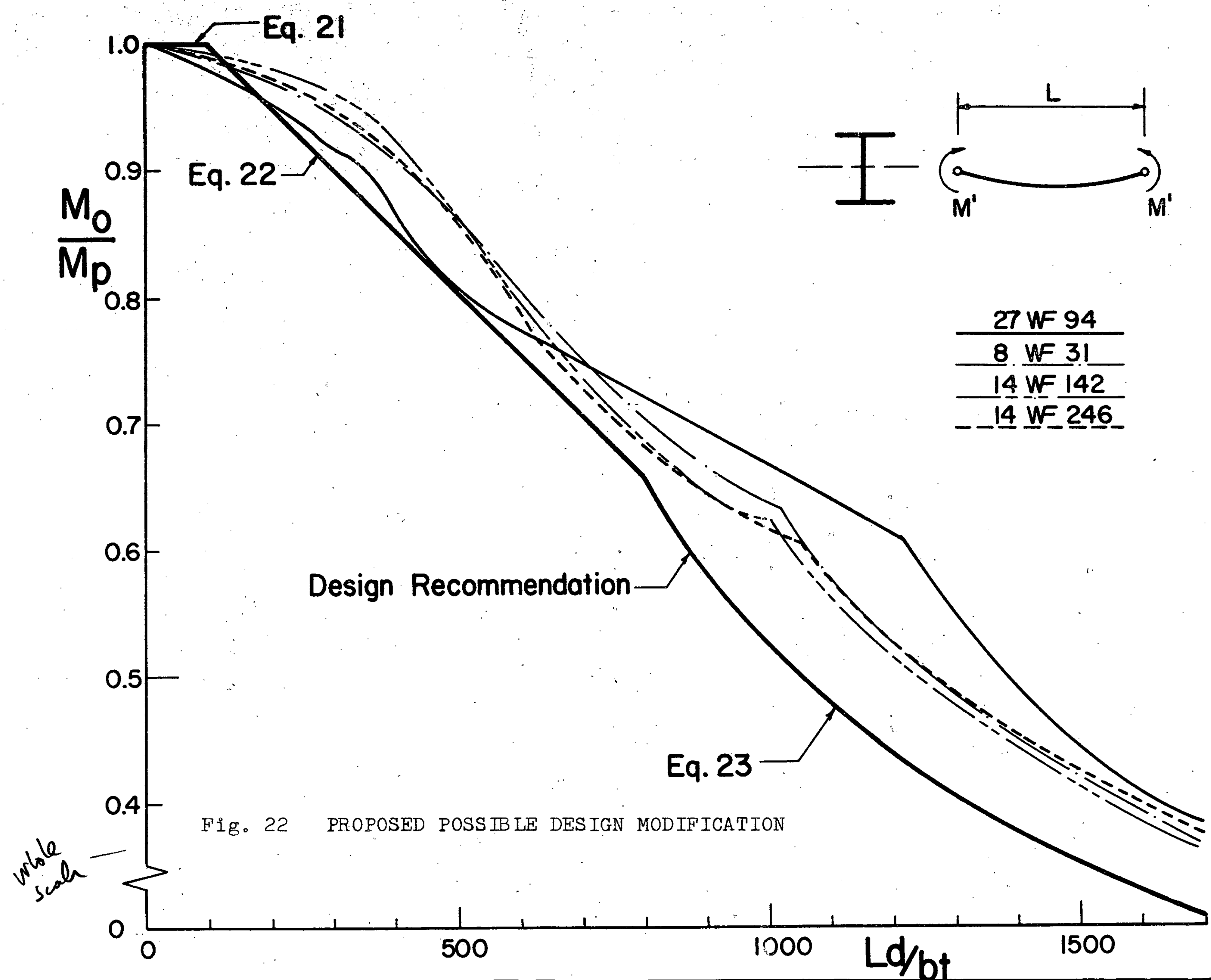

Fig. 22 PROPOSED POSSIBLE DESIGN MODIFICATION

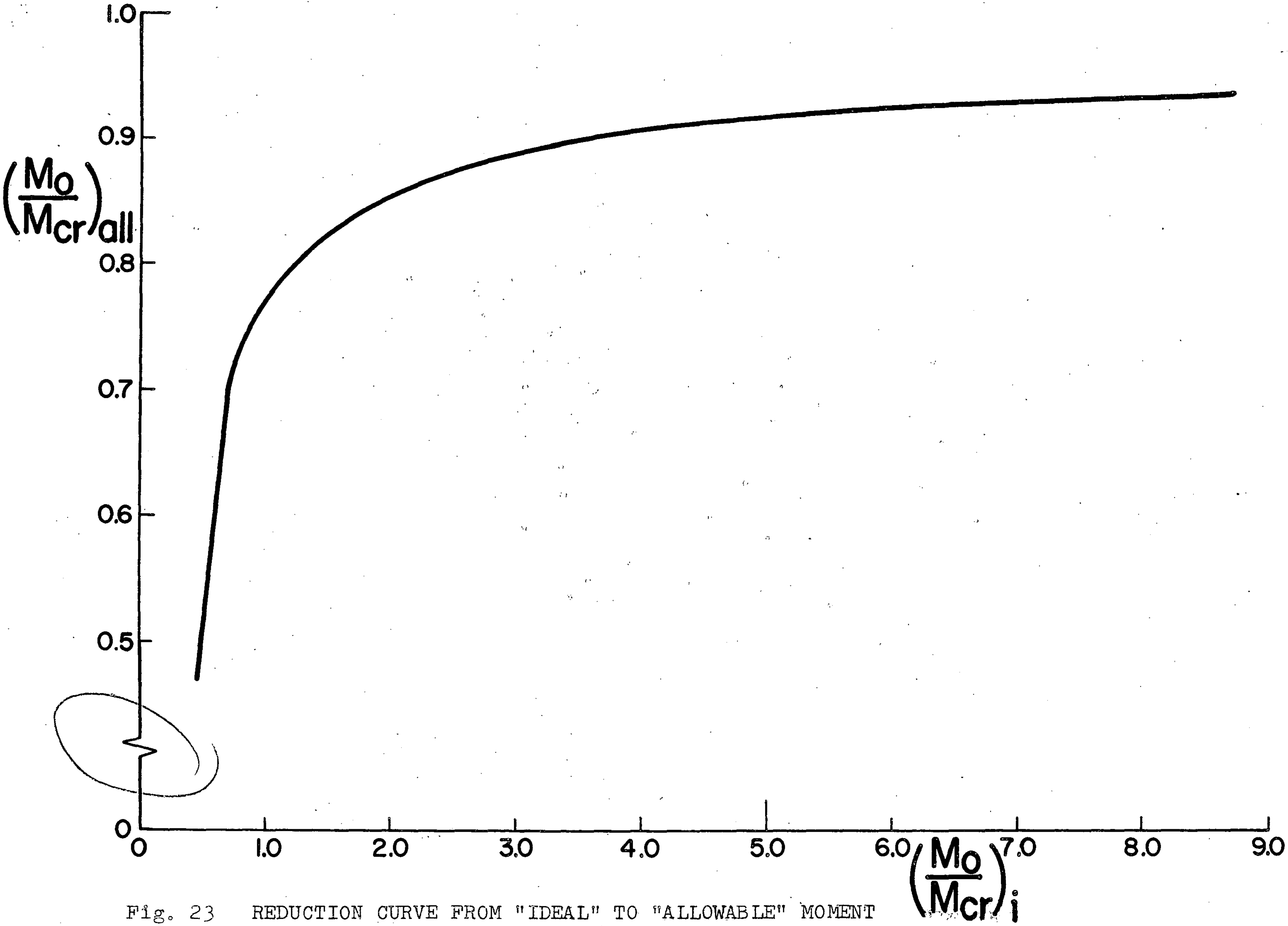

Fig. 23 REDUCTION CURVE FROM "IDEAL" TO "ALLOWABLE" MOMENT

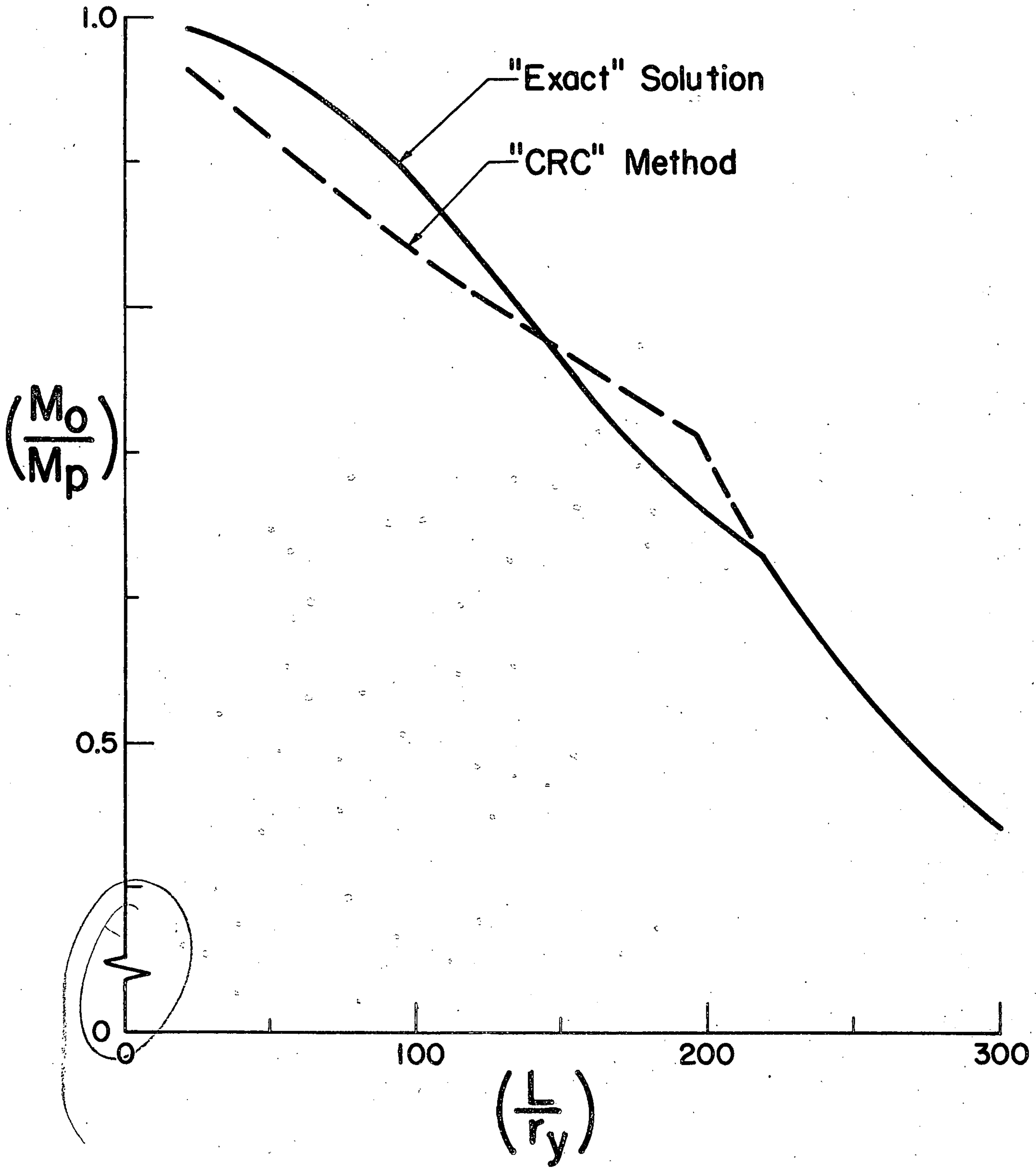

Fig. 24 COMPARISON BETWEEN "EXACT" SOLUTION AND "CRC" METHOD

REFERENCES

1. Bleich, F.
BUCKLING STRENGTH OF METAL STRUCTURES, McGraw-Hill Book Co., New York, 1952.

2. Lee, G. C.
LITERATURE SURVEY ON LATERAL INSTABILITY AND LATERAL BRACING REQUIREMENTS, Welding Research Council Bulletin 62, July 1960.

3. White, M. W.
THE LATERAL-TORSIONAL BUCKLING OF YIELDED STRUCTURAL STEEL MEMBERS, Ph.D. Dissertation, Lehigh University, 1956.

4. Wittrick, W. H.
LATERAL INSTABILITY OF RECTANGULAR BEAMS OF STRAIN HARDENING MATERIAL UNDER UNIFORM BENDING, Journal of Aeronautical Science, 19 (12), p. 835 (Dec. 1952).

5. Neal, B.G.
THE LATERAL INSTABILITY OF YIELDED MILD STEEL BEAMS OF RECTANGULAR CROSS SECTION, Philosophical Transactions of the Royal Society of London 242 (A) (Jan. 1950).

6. Horne, M. R.
CRITICAL LOADING CONDITIONS OF ENGINEERING STRUCTURES, Ph.D. Dissertation, Cambridge University, 1950.

7. Galambos, T. V.
INELASTIC LATERAL-TORSIONAL BUCKLING OF WIDE FLANGE COLUMNS, Ph.D. Dissertation, Lehigh University, 1959.

8. Haaijer, G.
PLATE BUCKLING IN THE STRAIN HARDENING RANGE, Transactions of the ASCE, 124, (2968) p.117 (1959).

9. Ketter, R. L.; Kaminski, E. L.; Beedle, L. S.
PLASTIC DEFORMATIONS OF WIDE-FLANGE BEAM-COLUMNS, Transactions of the ASCE, 120, (2772) p. 1028,(1955).

10. Timoshenko, S.
THEORY OF ELASTIC STABILITY, McGraw-Hill Book Co., New York, 1936.

11. Timoshenko, S.
STRENGTH OF MATERIALS, Vol. II, D. Van Nostrand Book Co., New York, 1948.

12. de Vries, K.
STRENGTH OF BEAMS AS DETERMINED BY LATERAL BUCKLING, Transactions of the ASCE, 112, p. 1245 (1947).

13. DIN 4114
GERMAN BUCKLING SPECIFICATIONS, 1953 (English Translation for CRC by T. V. Galambos and J. Jones, 1957).

14. AISC
STEEL CONSTRUCTION HANDBOOK, American Institute of Steel Construction.

15. CRC
GUIDE TO DESIGN CRITERIA FOR METAL COMPRESSION MEMBERS, Column Research Council, 1960.

16. Clark, J. W.; Hill, H. N.
LATERAL BUCKLING OF BEAMS, Proceedings of the ASCE, Proceedings Paper 2559 (ST7) p. 175, (July, 1960).

17. Galambos, T. V.; Ketter, R. L.
COLUMNS UNDER COMBINED BENDING AND THRUST, Proceedings of the ASCE, Proc. Paper 1990 (EM2) p. 1, (April, 1959).

18. AISC
PLASTIC DESIGN IN STEEL, American Institute of Steel Construction, 1959.

19. Lee, G. C.
INELASTIC LATERAL BUCKLING OF BEAMS AND LATERAL BRACING REQUIREMENTS, Ph.D. Dissertation, Lehigh University, 1960.